Journal of Medicinal Chemistry

Article

Identification of potent Ebola virus entry inhibitors with suitable properties for in-vivo studies

Hu Liu, Ye Tian, Kyungae Lee, Pranav Krishnan, May Kwang-Mei Wang, Sean Whelan, Emily Mevers, Veronica Soloveva, Benjamin Dedic, Xinyong Liu, and James Cunningham

J. Med. Chem., **Just Accepted Manuscript** • DOI: 10.1021/acs.jmedchem.8b00704 • Publication Date (Web): 19 Jun 2018

ACS Publications

is published by the American Chemical Society. 1155 Sixteenth Street N.W., Washington, DC 20036

Identification of potent Ebola virus entry inhibitors with suitable properties for *in-vivo* studies

Hu Liu,[2,#] Ye Tian,[1,3,#] Kyungae Lee,[2,§] Pranav Krishnan,[1] May Kwang-Mei Wang,[1] Sean Whelan,[2] Emily Mevers,[4] Veronica Soloveva,[5] Benjamin Dedic[1], Xinyong Liu,[3] and James M. Cunningham[1,2,*]

[1]*Division of Hematology, Department of Medicine, Brigham and Women's Hospital, Boston, MA 02115*

[2]*Department of Microbiology and Immunobiology, Harvard Medical School, Boston MA 02115*

[3]*Department of Medicinal Chemistry, Key Laboratory of Chemical Biology (Ministry of Education), School of Pharmaceutical Sciences, Shandong University, 44 West Culture Road, 250012 Jinan, Shandong, PR China*

[4]*Department of Biological Chemistry and Molecular Pharmacology, Harvard Medical School, Boston MA 02115*

[5]*United States Army Research Institute of Infectious Diseases, Fort Detrick MD 21702*

ABSTRACT: Previous studies identified an adamantane dipeptide piperazine **3.47** that inhibits Ebola virus (EBOV) infection by targeting the essential receptor Niemann-Pick C1 (NPC1). The physicochemical properties of **3.47** limit its potential for testing *in vivo*. Optimization by improving potency, reducing hydrophobicity, and replacing labile moieties, identified **3.47** derivatives with improved *in-vitro* ADME properties that are also highly active against EBOV infection, including when tested in the presence of 50% normal human serum (NHS). In addition, 3A4 was identified as the major cytochrome P450 isoform that metabolizes these compounds and accordingly, mouse microsome stability was significantly improved when tested in the presence of the CYP3A4 inhibitor ritonavir that is approved for clinical use as a booster of anti-HIV drugs. Oral administration of the EBOV inhibitors with ritonavir resulted in a pharmacokinetic profile that supports a b.i.d. dosing regimen for efficacy studies in mice.

KEY WORDS: Ebola virus, anti-viral, Niemann-Pick C1, cLogP, organic synthesis, ADME, pharmacokinetics

INTRODUCTION

Ebola virus (EBOV) is a highly pathogenic enveloped virus[1, 2] that caused the epidemic that began in the western African nation of Guinea in 2014 and spread to Liberia, Sierra Leone and Nigeria. During this outbreak, more than 28,000 people were infected and more than 11,000 died.[3, 4] The unpredictable onset, ease of transmission, rapid progression, and high morbidity and mortality of EBOV infection have created a high level of public concern that has led to focus on development of vaccines and anti-viral agents.[5-11]

Previously, we identified an adamantane piperazine dipeptide **3.47** that inhibited pseudotyped EBOV infection with an IC_{50} of 13 nM (**Figure 1**).[12, 13] Using genetic knockouts and biochemical assays utilizing a photo-affinity labelling analog **3.98**, the target of **3.47** was identified as the lysosome cholesterol transporter Niemann-Pick C1 (NPC1) expressed in susceptible cells.[12, 14] We found that **3.47** prevents infection by interfering with NPC1 binding[12, 13] and activation of the EBOV glycoprotein (GP) that mediates virus penetration into host cells.[12, 14] Recent studies have defined the role of NPC1 in more detail including reports of the atomic resolution structure of NPC1 bound to EBOV GP.[15, 16] Because NPC1 is essential for EBOV infection, **3.47** and its derivatives represent an attractive class of anti-viral agents.

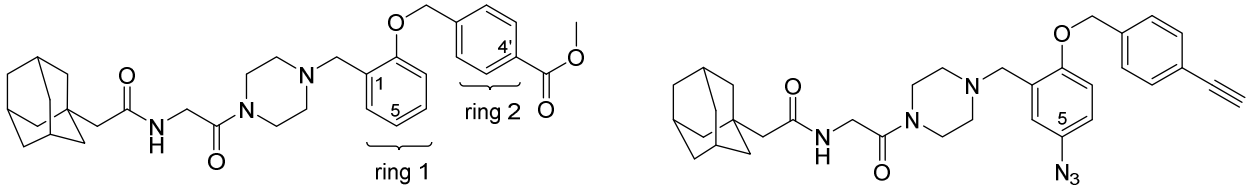

Figure 1. Adamantane dipeptide piperazines **3.47** and **3.98** are potent inhibitors of EBOV infection.

Although potent, **3.47** is hydrophobic (clogP = 7.2) and poorly soluble (kinetic solubility = 5 μM). In addition, the *in-vitro* ADME profile of **3.47** is sub-optimal. It is rapidly degraded by hepatic microsomes (**Table 1**) and contains a methyl ester that contributes to activity but is a target for hydrolysis. The current study is aimed at identifying potent **3.47** analogs that overcome

these liabilities and thus, are suitable for testing in animal models of EBOV infection. To achieve this goal, our approach has been to reduce hydrophobicity,[17, 18] and to modify metabolic "hot spots", such as the methyl ester and O-benzyl moieties.

Table 1. *In vitro* ADME properties of 3.47.

Compound	Kinetic Solubility	$T_{1/2}$ (mouse liver microsome)	$T_{1/2}$ (human liver microsome)
3.47	5.3 μM	1.0 min	1.2 min

CHEMISTRY

The syntheses of compounds **1a-1**, **1a-3**, **1a-4**, **1a-9** were previously reported.[13] Using similar methods, we synthesized compounds **1a-2**, **1a-5** to **8**, **1a-10** to **17** as illustrated in **Scheme 1**.

Scheme 1: General synthetic scheme for compounds **1a-2**, **1a-5** to **8**, **1a-10** to **17**.

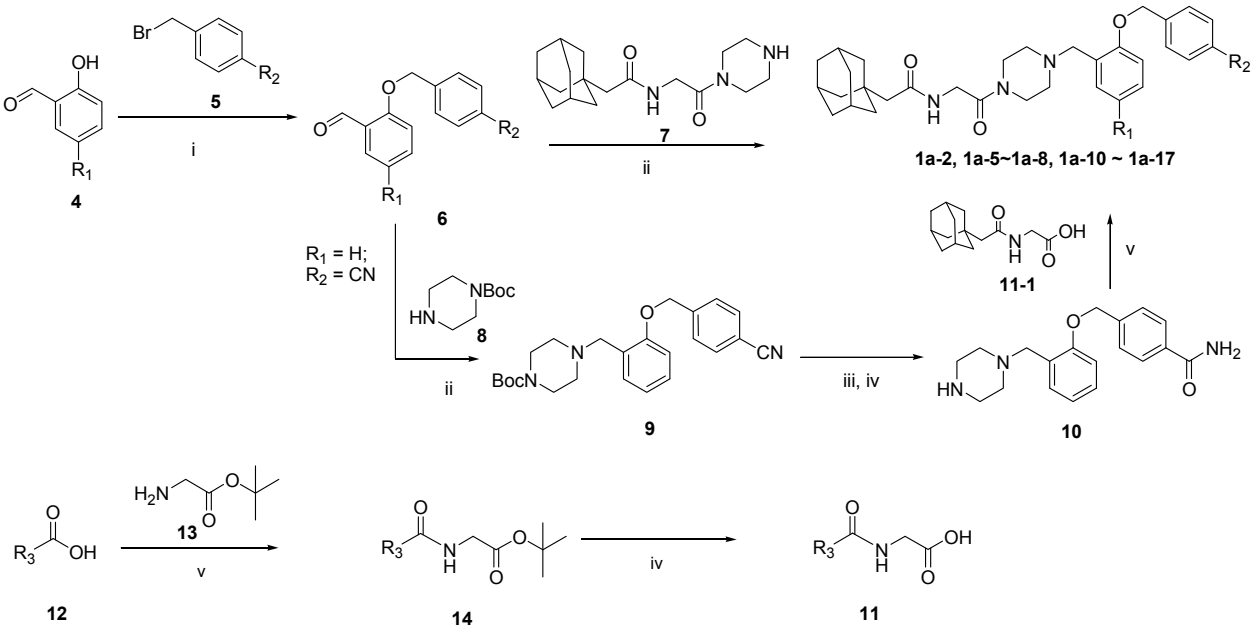

Reagents and conditions: (i) K_2CO_3, DMF, rt; (ii) $NaBH(OAc)_3$, DME or DCM, 0°C to rt;(iii) K_2CO_3, H_2O_2, DMSO; (iv) 4N HCl in dioxane, rt; (v) HATU or BOP, DIEA, DMF, rt.

Alkylation of the corresponding phenol **4** with the appropriate benzyl bromide gave benzyl ether **6** in good yields. Reductive amination with **7** (see **Scheme 5** for preparation) using sodium triacetoxyborohydride [$NaBH(OAc)_3$] gave the majority of compounds **1a** (**Scheme 1**), and either dimethoxy ethane (DME) or dichloromethane (DCM) as solvent worked well in these cases. For the 4-amide **1a-2**, reductive amination of corresponding **6** with Boc-protected piperazine, followed by standard acidic Boc deprotection, cyano hydrolysis to the primary amide, and amide coupling provided **1a-2**. The acid **11** was synthesized from appropriate acid **12** via amide coupling with *t*-butyl glycine ester **13**, followed by acidic *t*-butyl removal.

The synthesis of compounds **1a-18** and **1a-19** are depicted in **Scheme 2**. The cross-coupling reaction of 2-bromobenzaldehyde **15** and alkene **16** under the catalysis of palladium (II) acetate [$Pd(OAc)_2$], provided *trans*-alkene **17** which, followed by reductive amination, afforded

compound **1a-18**. The double bond was then reduced under standard hydrogenation conditions to provide compound **1a-19**.

Scheme 2: Synthetic scheme for compound **1a-18** and **1a-19**.

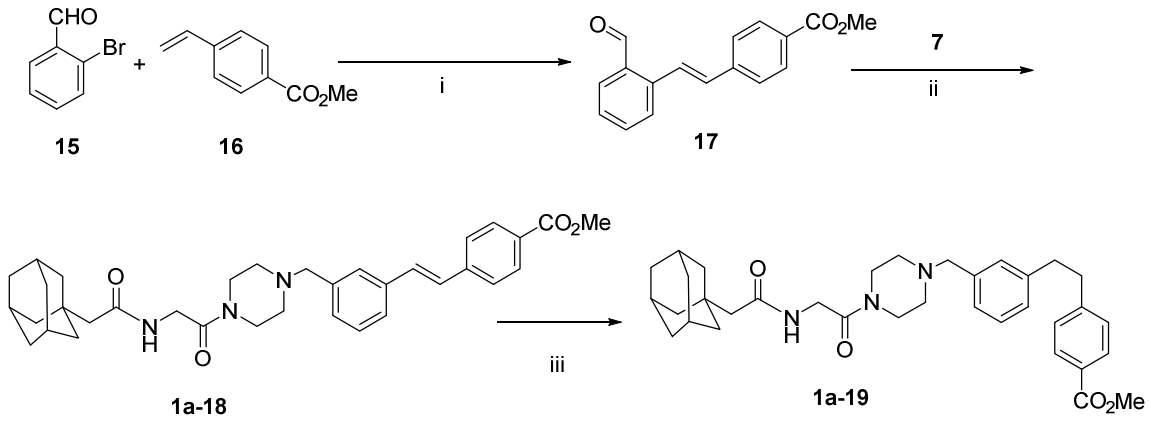

Reagents and conditions: (i) $Pd(OAc)_2$, Et_3N, $P(o\text{-}MeC_6H_4)_3$, Toluene, rt; (ii) $NaBH(OAc)_3$, DCM, 0 °C to rt; (iii) H_2, Pd/C, rt.

The synthesis of compound **1a-20** is shown in **Scheme 3**. The precursor bromide **18** was prepared similarly as shown in **Scheme 5**. Suzuki coupling of **18** using palladium(II) acetate [$Pd(OAc)_2$] and RuPhos as the ligand gave compound **1a-20**.

Scheme 3: Synthetic scheme for compound **1a-20**.

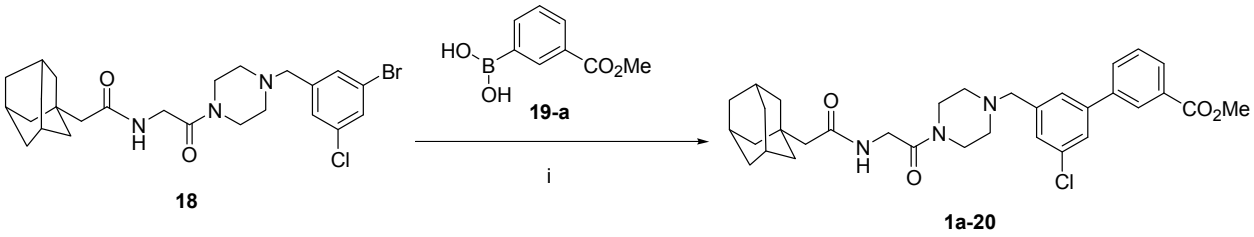

Reagents and conditions: (i) RuPhos, $Pd(OAc)_2$, KF, DME, 65 °C.

The synthesis of di-phenyl ether **1a-21** is shown in **Scheme 4**. Reacting aldehyde **20** with boc-piperazine **8** under the standard reductive amination conditions gave phenol **21**, which was then subjected to copper (II) acetate [$Cu(OAc)_2$]-promoted phenyl ether formation to afford compound **22**. Acidic Boc deprotection, followed by amide coupling with acid **11-1** provided **1a-21**.

Scheme 4. Synthetic scheme for compound **1a-21**.

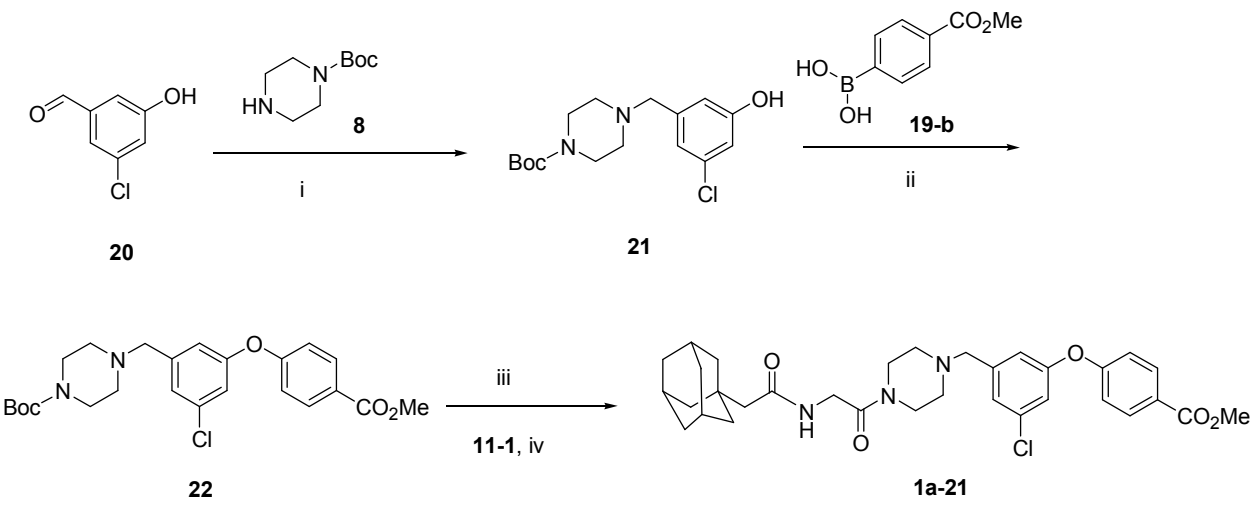

Reagents and conditions: (i) $NaBH(OAc)_3$, DCM, 0°C to rt;(ii) $Cu(OAc)_2$, Pyridine; (iii) 4N HCl in dioxane, rt; (iv) HATU, DIEA, DMF, rt.

Compounds in the small set of focused library (**1b-1** to **1b-18**) were synthesized as shown in **Scheme 5**. Coupling between adamantyl acetic acid **12-1** and glycine amide **23** gave **24** in good yield. Acidic Boc deprotection gave piperazine **7**, which upon treatment with different aldehydes **26** under the standard reductive amination conditions provided the crude products. Each crude product was further purified by acid-functionalized silica gel (Silica-$PhSO_3H$) column to afford **1b-1** to **1b-18** in greater than 90% purities.

Scheme 5. Synthetic scheme for compounds **1b-1** to **1b-18**.

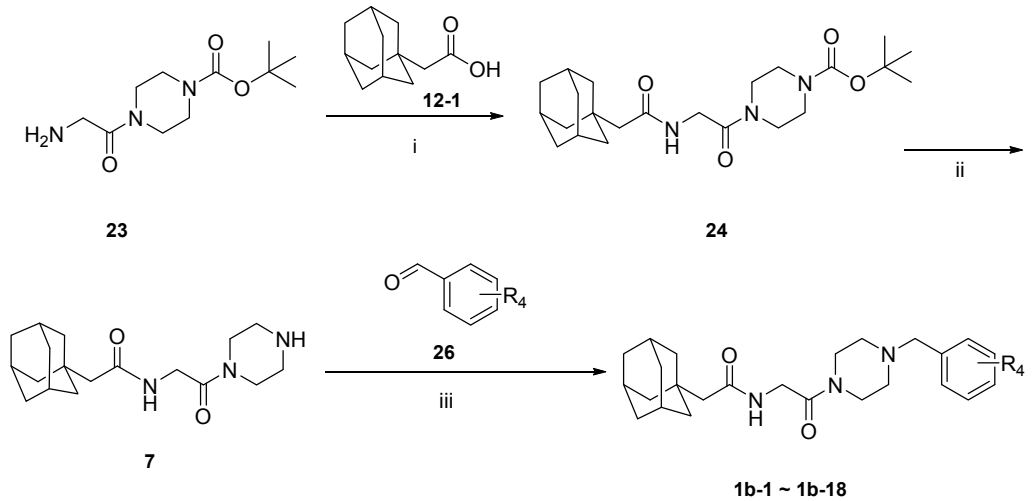

Reagents and conditions: (i) HATU, DIEA, DMF, rt; (ii) 4N HCl in dioxane, rt; (iii) $NaBH(OAc)_3$, DME or DCM, 0°C to rt.

The synthesis of compounds **2-1** to **2-18** is shown in **Scheme 6**. Similar to that described in **Scheme 1**, reductive amination of **6** with sodium triacetoxyborohydride [$Na(OAc)_3BH$] gave **27**. Standard acidic Boc deprotection, followed by amide coupling with Boc–protected glycine 2**9** provided **30**, which was then converted in two steps to **2-1** to **2-18**. Notably, the trifluoro(adamantan-1-yl)acetic acid **12-2** was obtained by a series of homologation reactions of commercially available **32**.

Scheme 6. Synthetic scheme for compounds **2-1** to **2-18**.

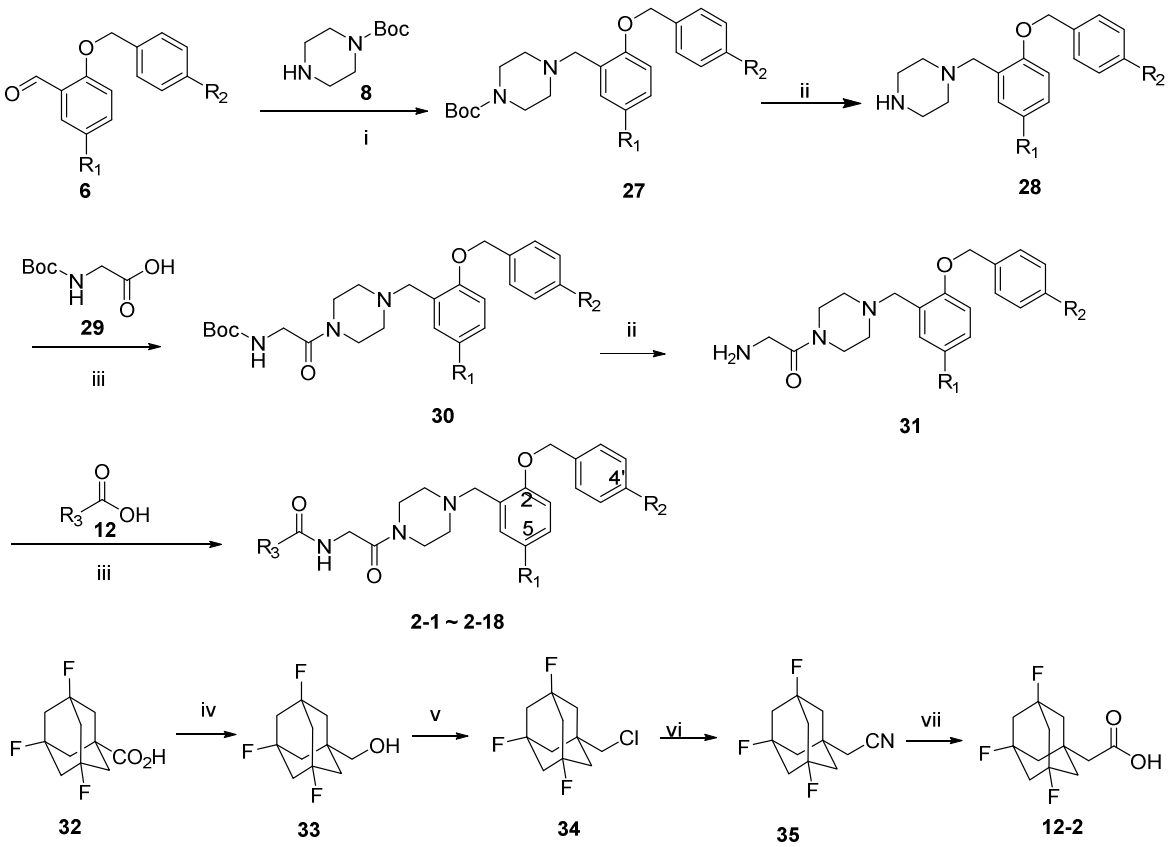

Reagents and conditions: (i) $NaBH(OAc)_3$, DME or DCM, 0°C to rt; (ii) 4N HCl in dioxane, rt; (iii) HATU, DIEA, DMF, rt; (iv) $LiAlH_4$, THF, 0°C to 65°C; (v) $SOCl_2$, DCE, 0°C to 70°C; (vi) NaCN, DMSO, 120 °C; (vii) KOH, $EtOH/H_2O$, 75°C.

The synthesis of compounds **3-1** to **3-7**, **3-10** to **3-13** are shown in **Scheme 7**. Both reactants, piperazine **37** and the glycine piperazine amide **38,** were prepared similarly as compounds **28** or **31** respectively, as described in **Scheme 6**. Coupling of **37** or **38** with the corresponding acids **11** or **12**, using 1-ethyl-3-(3-dimethylaminopropyl)carbodiimide (EDCI), afforded compounds **3-1** to **3-7**, **3-10** to **3-13**. It is noteworthy to point out that, for either reactants **37** or **38** with a free

amino NH_2 as the R_4 group such as in compound **3-6**, amide coupling with acids **11** or **12** under the HATU conditions gave a significant amount of bis-acylated side product (with the 2nd acylation at the aniline NH_2), and this issue was alleviated largely using EDCI conditions.

Scheme 7. Synthetic scheme for compounds **3-1** to **3-7**, **3-10** to **3-13**.

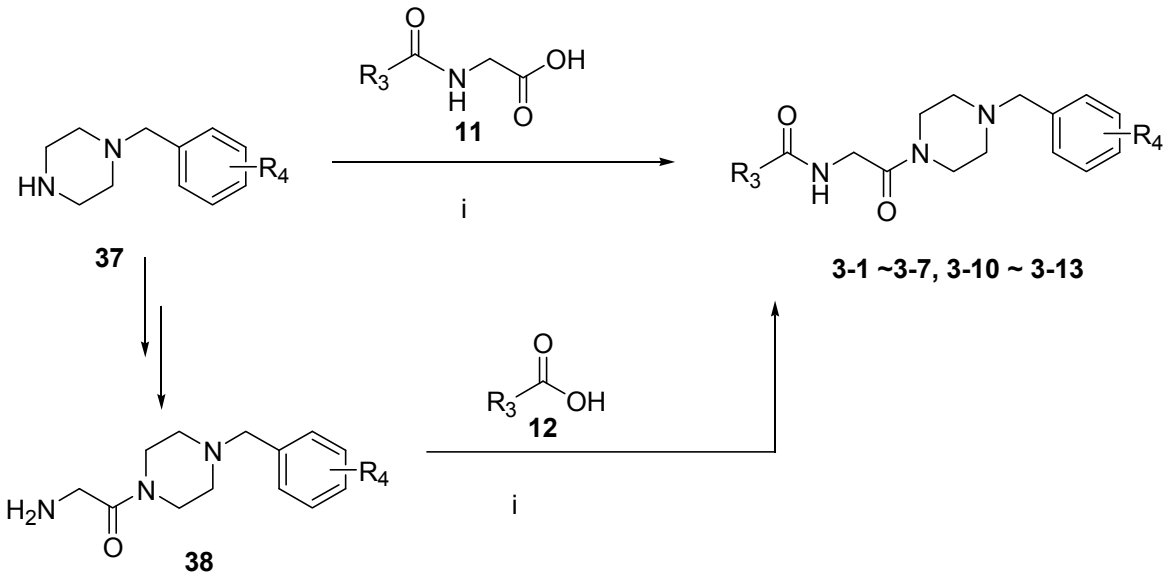

Reagents and conditions: (i) EDCI, HOBt, DIEA, DCM, rt.

The synthesis of compounds **3-8**, **3-9** and **3-14** are shown in **Scheme 8**. The intermediates **40** and **43** were prepared similarly as described in **Scheme 6**, using the standard reductive amination conditions. Acylation or sulfonylation of **40**, or cyclopropane replacement of the bromide in **43** via Suzuki coupling, afforded intermediates **41** and **44** respectively, which were converted to compounds **3-8**, **3-9** and **3-14** via acidic Boc removal, followed by EDCI-promoted amide coupling.

Scheme 8. Synthetic scheme for compounds **3-8**, **3-9** and **3-14**.

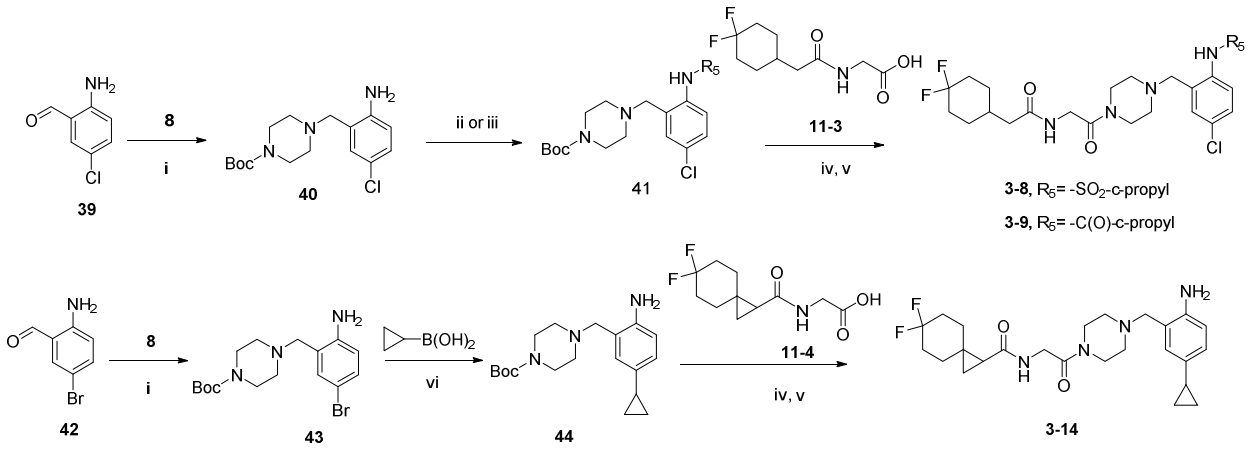

Reagents and conditions: (i) $NaBH(OAc)_3$, DME or DCM, 0°C to rt; (ii) Cyclopropanesulfonyl chloride, pyrimidine, DCM, rt **(for 3-8)**; (iii) Cyclopropanecarbonyl chloride, TEA, DCM, rt (**for 3-9**); (iv) 4N HCl in dioxane, rt; (v) EDCI, HOBt, DIEA, rt; (vi) K_3PO_4, $(C_6H_{11})_3P$, $Pd(OAc)_2$, $PhMe/H_2O$), 80°C.

The synthesis of compounds **3-15** to **3-17** are shown in **Scheme 9**. Acylation of piperazine **8** with cyclic anhydride **45** gave **46** with a high yield. After standard acidic Boc removal, the amide in **47** was reduced by $LiAlD_4$ to afford deuterated **48**. From intermediates **47** or **48**, compounds **3-15** to **3-17** were prepared similarly as described in **Scheme 8**.

Scheme 9. Synthetic scheme for compounds **3-15** to **3-17**.

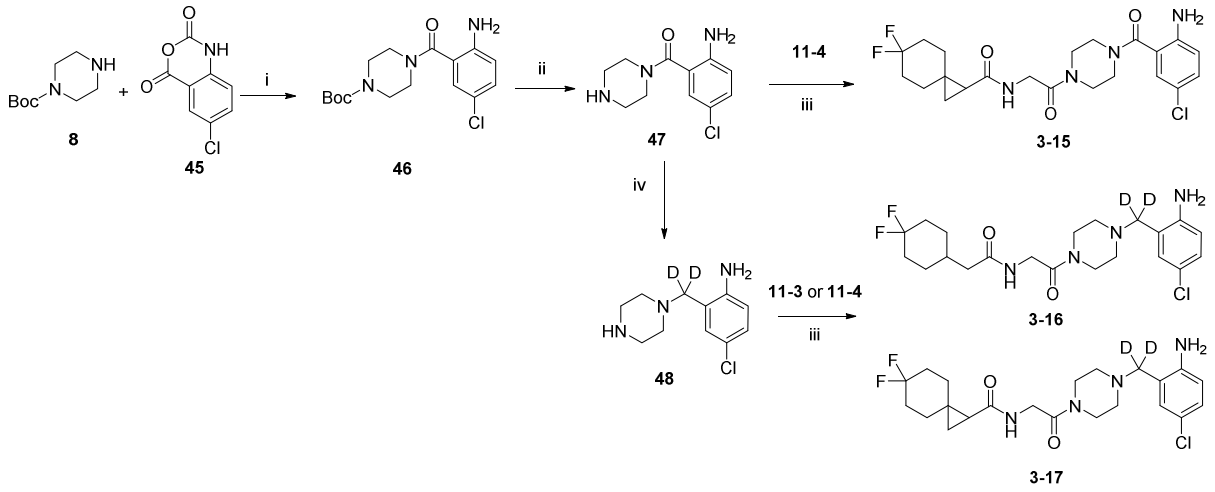

Reagents and conditions: (i) DMAP, DMF, rt; (ii) 4N HCl in dioxane, rt; (iii) EDCI, HOBt, DIEA, DCM, rt; (iv) $LiAlD_4$, THF, 0°C to 65 °C.

The synthesis of compounds **3-20** and **3-21** are illustrated in **Scheme 10**. Aldehyde **6-1**, prepared similarly as in **Scheme 1**, was treated with glycine attached piperazine **49** under

standard reductive amination condition to afford **30-1** in good yield. Boc removal, followed by EDCI-promoted amide coupling, gave compounds **3-20** and **3-21**.

Scheme 10. Synthetic scheme for compounds **3-20** and **3-21**.

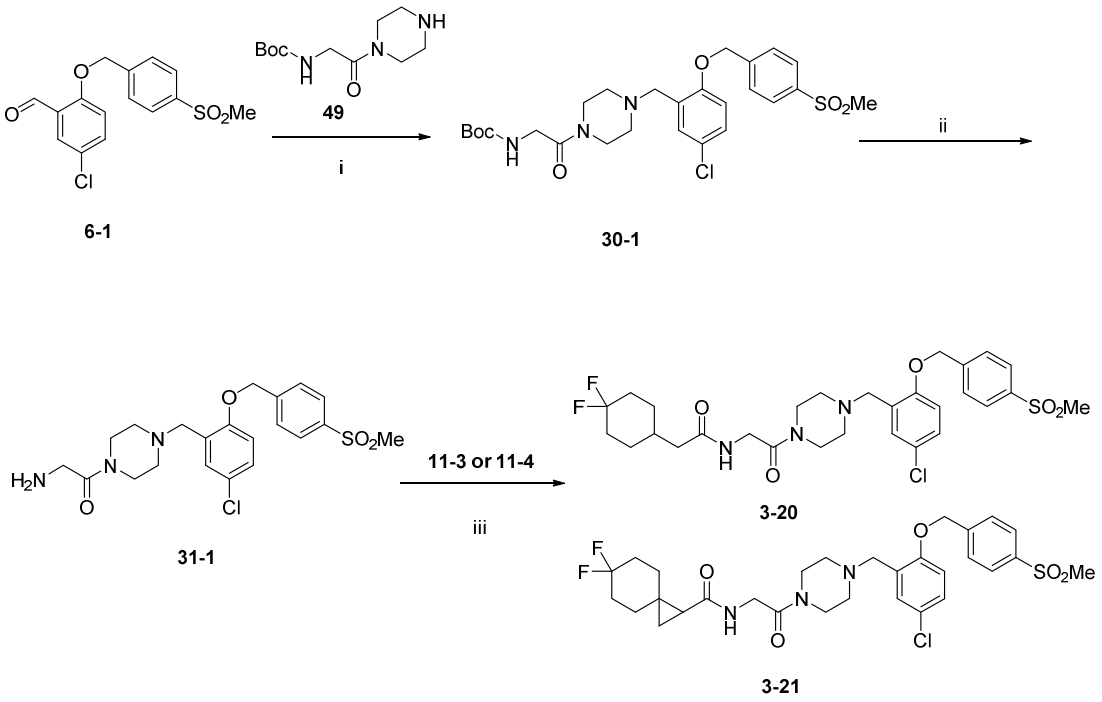

Reagents and conditions: (i) $NaBH(OAc)_3$, DME or DCM, 0°C to rt; (ii) 4N HCl in dioxane, rt; (iii) EDCI, HOBt, DIEA, DCM, rt.

The syntheses of compounds **3-23**, **3-24** and *(-)***3-25** are shown in **Scheme 11**. Compounds **3-6**, **3-10** and *(-)***3-18** were converted to compounds **3-23**, **3-24** and *(-)***3-25** smoothly upon treatment with 4-methylsulfonyl benzaldehyde **26-1** under reductive amination conditions.

Scheme 11. Synthetic scheme for compounds **3-23**, **3-24** and *(-)***3-25**.

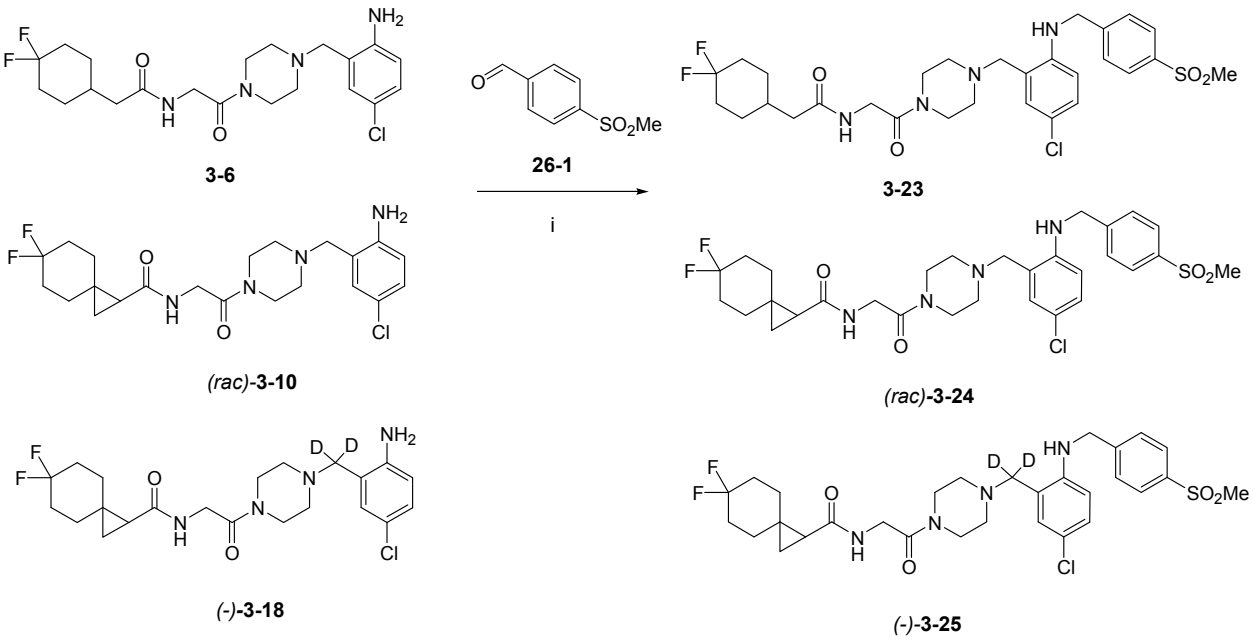

Reagents and conditions: (i) $NaBH(OAc)_3$, DME or DCM, 0°C to rt.

RESULTS AND DISCUSSION

The initial goal was to identify functional groups to replace the labile 4'-methyl ester in **3.47** (**Table 2**). The activities of analogs containing various 4'-substitutions were measured by testing their effects on infection of Vero cells by vesicular stomatitis virus (VSV) particles pseudotyped with EBOV GP.[19]

Table 2. Replacement of the methyl ester in compound 3.47.

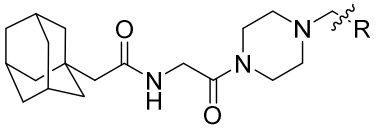

1a

No.	R	IC_{50} (nM)[a]
3.47	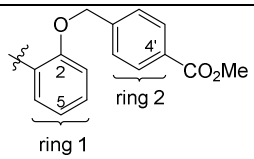	13

1a-1	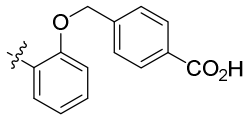	4000[b]
1a-2	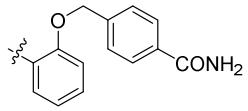	700
1a-3	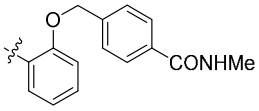	2100[b]
1a-4	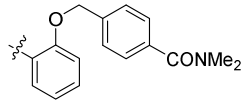	3300[b]
1a-5	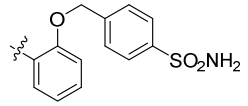	350
1a-6	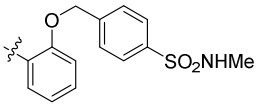	300
1a-7	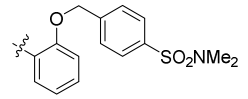	400
1a-8	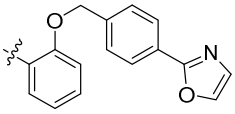	270
1a-9	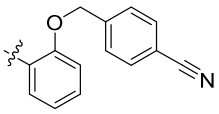	4400[b]
1a-10	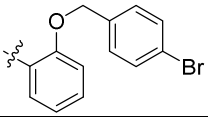	220

[a]IC_{50}: concentration of compound required to inhibit VSV EBOV infection of Vero cells by 50%.

[b]: Data from our previous reported work.[13]

As expected, we found that the **3.47** hydrolysis product **1a-1** containing the 4'-carboxylic acid is significantly less active than **3.47**. Replacement of the ester with amides or sulfanamides (compounds **1a-2** to **1a-7**) reduced the cLogP, but also the potency. The bioisosteric oxazole **1a-8** is only moderately active (IC_{50} = 270 nM), binds tightly to mouse plasma proteins (99.7%) and is rapidly degraded by mouse microsomes ($T_{1/2}$ = 1 min). In addition, **1a-8** is also unstable in mouse plasma, suggesting that one or more of the amide bonds is also sensitive to hydrolysis (**Table 10**).

In addition, we also examined the substitution pattern on phenyl ring 1. Previous SAR that led to the design of the 5-azido crosslinker **3.98** (**Figure 1**) indicated that substitutions at the 5 position might be beneficial for anti-viral activity.[12, 13]

Table 3. 5-Substituted phenyl ring 1 and methyl sulfone as the replacement for the ester.

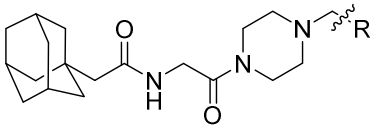

1a

No.	R	IC_{50} (nM)[a]
1a-11	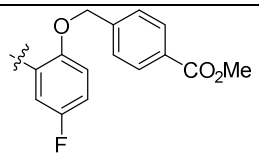	1.4
1a-12	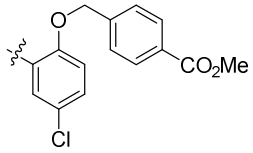	1.1
1a-13	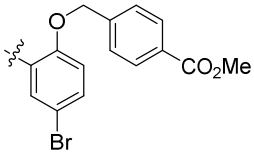	9
1a-14	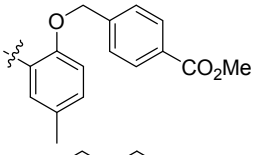	12
1a-15	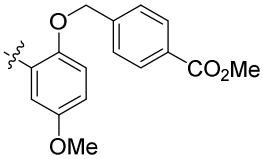	1400
1a-16	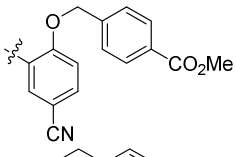	50
1a-17	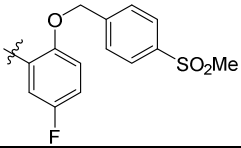	5

[a]IC_{50}: concentration of compound required to inhibit VSV EBOV infection of Vero cells by 50%.

Indeed, we found that 5-substitution with fluorine (**1a-11**, IC_{50} =1.4 nM**)** or chlorine (**1a-12** IC_{50} = 1.1 nM) improved anti-viral activity by almost ten-fold with the 5-chloro being slightly preferred (**Table 3**). This suggests that the 5-halo group occupies a small yet crucial hydrophobic pocket in NPC1. Taking advantage of this new finding, further studies demonstrated that substitution of methyl sulfone for the carboxymethyl in **1a-11** did not substantially affect the potency of the product **1a-17** (IC_{50} = 5 nM). Thus, compared to **3.47**, **1a-17** is more potent, less hydrophobic (cLogP = 5.8) and lacks the unstable carboxymethyl ester.

In addition to the methyl ester, the O-benzyl moiety is also a potential site for oxidative metabolism. Taking this into account, we examined the possibilities of replacing this moiety.

Table 4. Substitutions for the O-benzyl moiety.

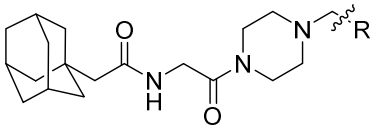

1a

No.	R	IC_{50} (nM)[a]
1a-18	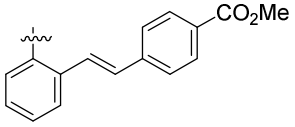	1500
1a-19	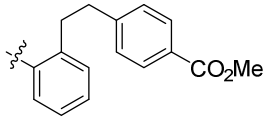	20
1a-20	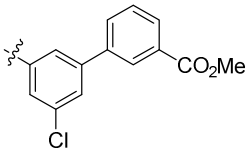	250
1a-21	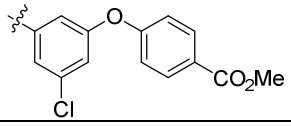	16

[a]IC_{50}: concentration of compound required to inhibit VSV EBOV infection of Vero cells by 50%.

Replacement of the O-benzyl with a more rigid *trans*-double bond markedly reduced activity (**Table 4**, **1a-18**, IC_{50} = 1500 nM). In contrast, **1a-19**, which has a saturated carbon-carbon linkage, is only slightly less potent than **3.47**, suggesting that for compounds like **3.47** or **1a-19**

in which the linkage between the two phenyl rings is able to rotate, the most active conformation is the *pseudo-cis* conformation. Modelling studies indicated that if this is correct, the labile O-benzyl linkage might be successfully replaced by a single bond (**1a-20**) or by an ether linkage (**1a-21**). Testing of these compounds revealed that **1a-20** suffered a significant loss of potency (IC_{50} = 250 nM). However, the ether linkage was much better tolerated (**1a-21**, IC_{50} =16 nM). This strongly suggests that the ether-linked methyl benzoate in **1a-21** fills the same binding pocket occupied by the phenyl ring 2 of **3.47**.

Encouraged by the finding that the O-benzyl linkage might not be critical for activity, we synthesized and tested focused libraries of derivatives in which the O-benzyl is absent. Representative results of this line of investigation are summarized in **Table 5**.

Table 5. Removal of the O-benzyl ring 2.

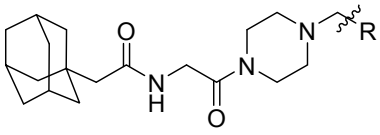

1b

No.	R	IC_{50} (nM)[a]	No.	R	IC_{50} (nM)[a]
3.0	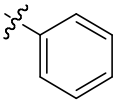	1300[b]	**1b-10**	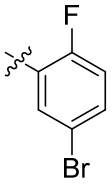	1200
1b-1	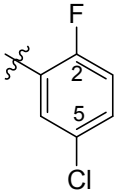	360	**1b-11**	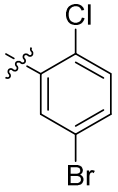	2200
1b-2	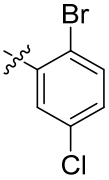	1050	**1b-12**	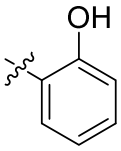	2900[b]
1b-3	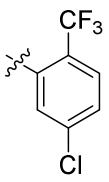	> 2000	**1b-13**	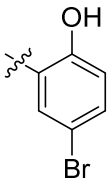	500

1b-4	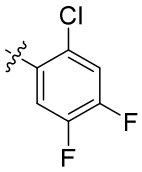	1450	**1b-14**	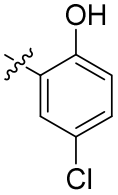	200
1b-5	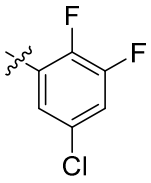	670	**1b-15**	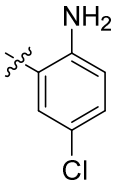	90
1b-6	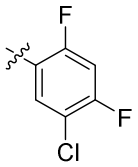	370	**1b-16**	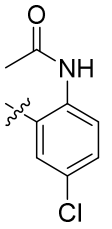	950
1b-7	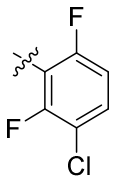	1350	**1b-17**	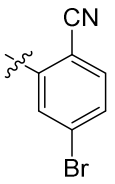	310
1b-8	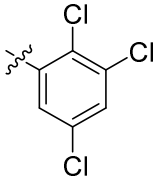	430	**1b-18**	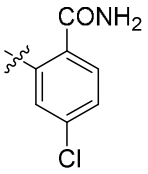	1900
1b-9	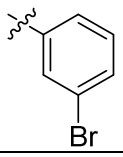	1000[b]			

[a]IC_{50}: concentration of compound required to inhibit VSV EBOV infection of Vero cells by 50%.

[b]: Data from our previous reported work.[13]

The analysis revealed that replacement of the 2-oxy benzyl moiety with hydrophobic groups such as halogens and -CF_3 (**1b-1** to **1b-3**) markedly reduced anti-viral activity. Tri-halo substitutions on ring 1 such as **1b-4** to **1b-8** were also weakly active. Interestingly, we found that although the 2-OH-containing compound **1b-12** (IC_{50} = 2900 nM) and the 3-bromo **1b-9** (IC_{50} = 1000 nM) are only moderately active, combining these modifications into one single molecule **1b-13** markedly improved potency (IC_{50} = 500 nM). Moreover, substitution of chloride for the 5-bromo further increased activity (**1b-14**, IC_{50} = 200 nM). A number of other polar substitutions at the 2-position were also explored (**1b-15** to **1b-18**). Among them, we found that the 2-NH_2-

substituted **1b-15** is even more potent (IC_{50} = 90 nM) and less hydrophobic (cLogP = 5.2) than the 2-OH in **1b-14** (IC_{50} = 200 nM; cLogP = 5.80). This suggests that a polar interaction between the 2-OH or 2-NH_2 and NPC1 places the 5-halogen in a favorable position to occupy the crucial hydrophobic pocket in NPC1.

With the progress achieved in replacing the labile moieties and reducing the hydrophobicity of the right-hand side, such as **1a-17** and **1b-15**, we focused on modification or replacement of the adamantane moiety (**Table 6**). Tri-fluoro substitution of the adamantane (compound **2-3**) maintained activity but failed to improve microsome stability (**Table 10**). Not surprisingly, addition of polar moieties to the adamantane, such as compounds **2-6** and **2-7**, also reduced anti-viral activity, confirming that the binding environment around the adamantane is hydrophobic.

Table 6. Modifications of and substitutions for the adamantane.

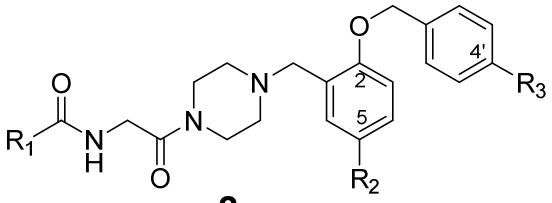

2

No.	R_1	R_2	R_3	IC_{50} (nM)[a]
2-1	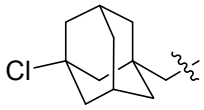	H	Br	500
2-2	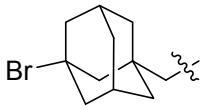	H	Br	600
2-3	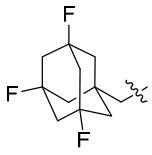	H	Br	200
2-4	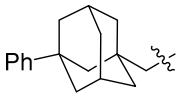	H	Br	700
2-5	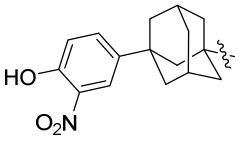	H	Br	600

2-6	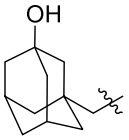	H	Br	500
2-7	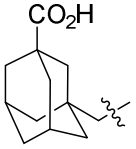	H	CO_2Me	> 2000
2-8	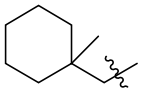	H	Br	520
2-9	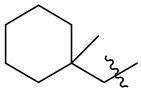	H	CO_2Me	80
2-10	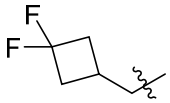	H	CO_2Me	300
2-11	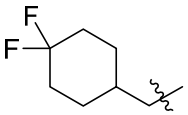	H	CO_2Me	50
2-12	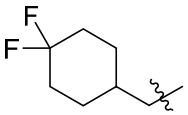	F	CO_2Me	18
2-13	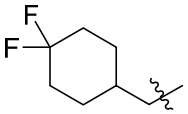	Cl	CO_2Me	15
2-14	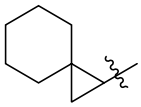	H	CO_2Me	73
2-15	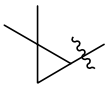	H	CO_2Me	300
2-16		H	CO_2Me	2900
2-17	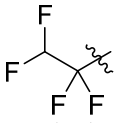	Cl	CO_2Me	160
2-18	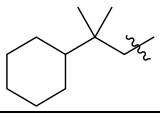	H	Br	> 2000

[a]IC_{50}: concentration of compound required to inhibit VSV EBOV infection of Vero cells by 50%.

Previously, we found that replacement of the adamantane with an unsubstituted cyclohexaneacetamide was poorly tolerated (>30-fold loss of activity).[13] Gratifyingly, further studies revealed that functionalized cyclohexanes could be effective replacements. For example,

the methyl-substituted cyclohexane **2-9** has an IC_{50} of 80 nM. Other preferred cyclohexanes include the 4,4-di-fluoro-cyclohexane **2-11** (IC_{50} = 50 nM), and the spiro-cyclopropane-cyclohexane **2-14** (IC_{50} = 73 nM). By contrast, the di-fluoro-cyclobutane in compound **2-10** does not seem to have sufficient size to fill the adamantane-binding pocket in NPC1. We also tested whether the cyclopropane ring alone, as in **2-14**, was adequate to achieve desired potency, and found that neither **2-15** (IC_{50} = 300 nM) nor **2-16** (IC_{50} = 2900 nM) exhibited significant activity. Importantly, we confirmed that the halogen substitutions at the 5-position of phenyl ring 1 further improved the anti-EBOV activity of compounds **2-12** (IC_{50} = 18 nM) and **2-13** (IC_{50} = 15 nM). Thus, successful replacement of the adamantane resulted in potent inhibitors with significantly lower cLogPs than **3.47** (**2-12**, clogP = 5.16 and **2-14**, clogP = 5.42).

To identify the most promising compounds for advancement, we evaluated derivatives that contained the optimized functional groups (**Table 7**).

Table 7. 2-Amino or -hydroxyl benzyl-piperazinyl-2-(4,4-difluoro-cyclohexyl)-acetamides.

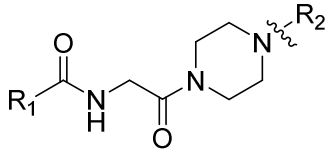

3

No.	R_1	R_2	IC_{50} (nM)[a]
3-1	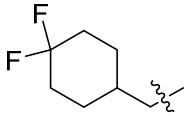	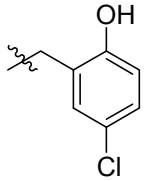	470
3-2	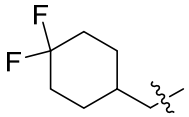	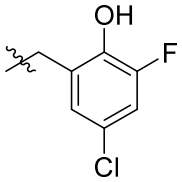	2800
3-3	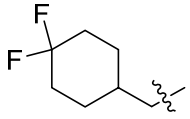	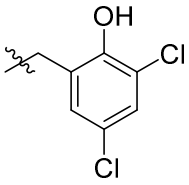	3600

3-4	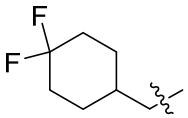	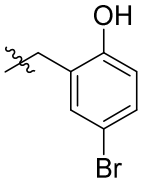	790
3-5	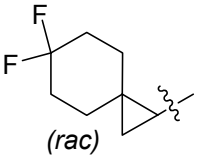	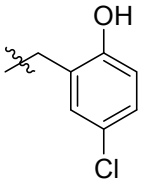	180
3-6	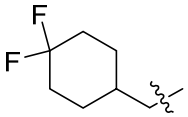	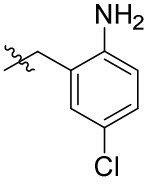	340
3-7	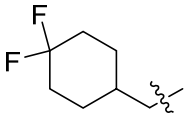	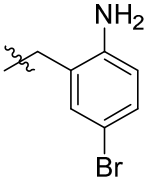	1740
3-8	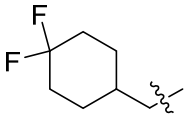	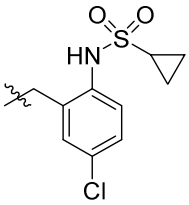	2200
3-9	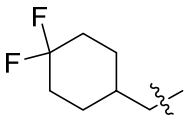	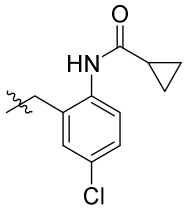	3500
3-10	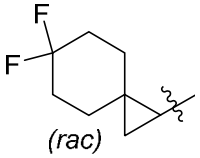	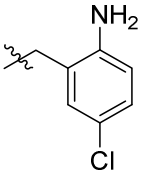	100
3-11	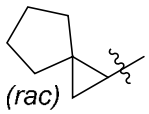	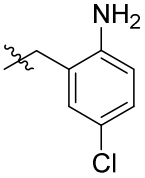	240
3-12	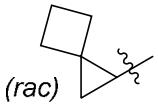	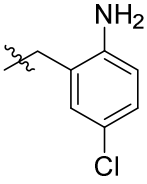	2500

3-13	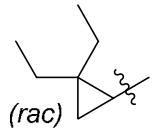	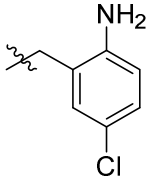	160
3-14	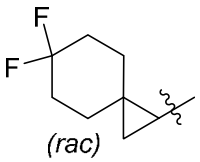	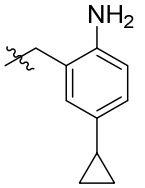	4200
3-15	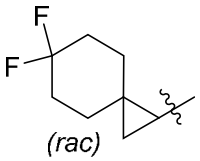	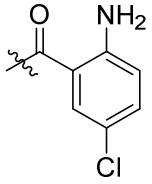	>5000
3-16	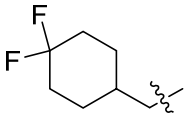	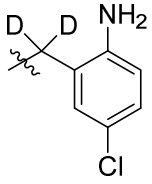	347
3-17	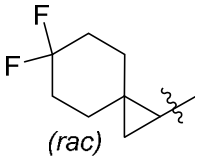	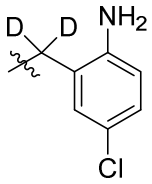	94
3-18	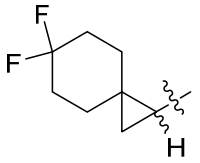	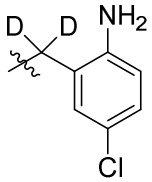	51
3-19	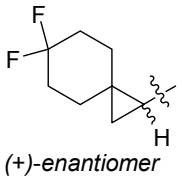	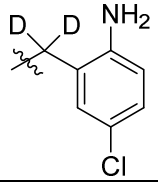	180

[a]IC_{50}: concentration of compound required to inhibit VSV EBOV infection of Vero cells by 50%.

We found that compound **3-1** containing the di-fluoro-cyclohexane acetamide replacement for adamantane and the 2-OH, 5-Cl substituted phenyl ring 1 has an IC_{50} of 470 nM. As previously found, substitutions at other positions on ring 1 were deleterious (**3-2** and **3-3**). Importantly, incorporation of the spiro-cyclopropane into **3-1** significantly increased potency (**3-5**, IC_{50} = 180

nM), indicating that the 4,4-difluoro-cyclohexane spiro-cyclopropane combination is the preferred replacement for the adamantane. As expected, replacement of 2-OH in **3-5** with 2-NH_2 was beneficial (**3-10**, IC_{50} = 100 nM). Moderate loss of potency was observed when the di-fluoro-substituted cyclohexane was replaced by cyclopentane, and further reductions in the ring size were even more deleterious (**3-11** and **3-12**). Interestingly, **3-11** and **3-13** possess similar potencies, with **3-13** being the open ring analog of the former. We also tested **3-16** and **3-17**, two derivatives of **3-6** and **3-10**, in which the benzylic position is blocked with deuterides,[20] and found this modification had little impact on potency. Since the cyclopropane has a chiral center, the racemic **3-17** was separated into the enantiomers, *(-)*-**3-18**, and *(+)*-**3-19**. We found that *(-)*-**3-18** (IC_{50} = 51 nM) is 3-fold more potent than *(+)*-**3-19** (IC_{50} = 180 nM).

We also evaluated the effect of adding the benzyl moiety to scaffolds such as phenols **3-1** and **3-5**, and anilines **3-6**, **3-10** and **3-18 (Table 8)**. We found that the 2-O-benzyl analogs are more potent than **3.47** (IC_{50} = 63 nM), with the enantiomer *(-)*-**3-22** being the most active (IC_{50} = 19nM). Similarly, the 2-NH benzyl derivatives (**3-23** to **3-25**) showed the same trend, with *(-)*-**3-25** being the most potent **(**IC_{50} = 21 nM). These studies were carried out utilizing the replication competent VSV vector rVSV[14]. Compared to pseudotyped VSV, rVSV is slightly less susceptible to inhibition but significantly more stable when studied in cells cultured in medium containing high serum to mimic *in vivo* conditions. Studies using this virus demonstrated that the potencies of **3-22** and of **3-25** were reduced by only 5-fold when tested in media containing 10% fetal bovine serum with 50% normal human serum.

Table 8. Evaluation of benzyl containing NPC1 inhibitors.

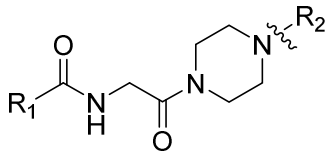

3

No.	R_1	R_2	IC_{50} (nM)[a]	IC_{50} (nM)[b]
3.47	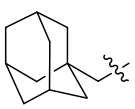	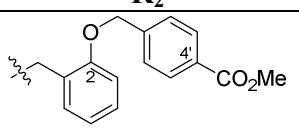	64	-

3-16	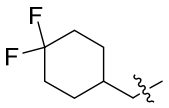	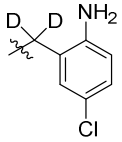	1195	-
3-18	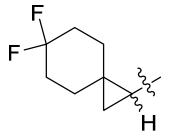 *(-)-enantiomer*	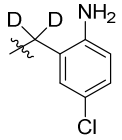	163	-
3-20	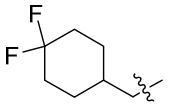	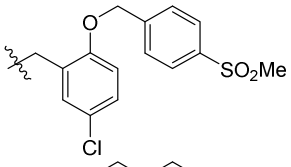	38	-
3-21	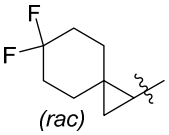 *(rac)*	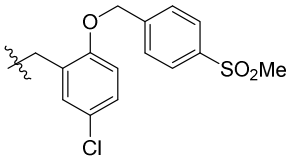	35	-
3-22	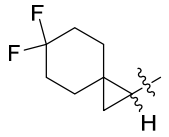 *(-)-enantiomer*	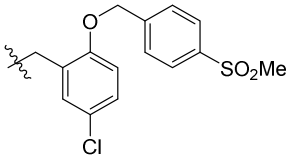	19	93
3-23	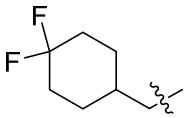	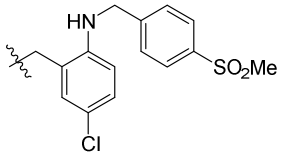	28	-
3-24	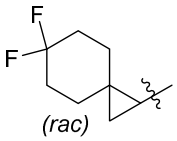 *(rac)*	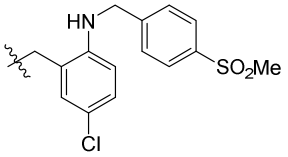	40	
3-25	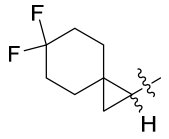 *(-)-enantiomer*	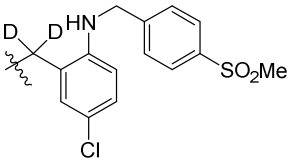	21	109

[a]IC_{50}: concentration of compound required to inhibit rVSV EBOV infection of Vero cells by 50%.

[b]IC_{50}: concentration of compound required to inhibit VSV EBOV infection of Vero cells by 50% in the presence of media containing 10% FBS and 50% NHS.

Although the aniline, as in **3-18**, **3-23** to **3-25**, is considered a structural alert,[21] the high fatality rate and short duration of treatment of EBOV infection may mitigate this concern.

We compared the activities of **3.47**, **3-21, 3-23** and **3-24** on the growth of *bona fide* EBOV **(Table 9)**. This test measured the effect of these inhibitors on virus production by HeLa cells for

two days after infection with EBOV isolates Mayinga (1976), Kikwit (1995) and Makona (2014) that caused the three largest outbreaks in Africa. We found that **3-23** and **3-24** are substantially more active than **3.47** against these viruses. Under these conditions, the concentration of these inhibitors that are required to reduce cell viability by 50% exceeded 10 μM. These findings demonstrate that the VSV EBOV entry assay is a reasonable predictor of activity against *bona fide* EBOV.

Table 9. Inhibition of EBOV growth in Hela cells.

No.	EC_{50} (nM) EBOV Kikwit	EC_{50} (nM) EBOV Makona	EC_{50} (nM) EBOV Mayinga
3.47	280	160	590
3-21	210	140	420
3-23	12	52	33
3-24	9	17	35

We examined the impact of replacement of the adamantane and other changes that decreased hydrophobicity on the *in vitro* ADME properties of **3-6** (clogP = 2.94)**, 3-16** (clogP = 2.94)**, 3-18** (clogP = 2.87)**, 3-20** (clogP = 4.10)**, 3-22 (**clogP = 3.82) and **3-25 (**clogP = 3.24) (**Table 10**). Although inhibitors **3-22** and **3-25** are very potent, they are less soluble and bind more extensively to mouse plasma proteins (plasma protein binding, PPB = 97.6% and 99.8%, respectively) than smaller compounds such as **3-6**, and **3-18 (**PPB = 86.9% and 87.9%, respectively). The stability of each compound in plasma is determined by factors such as the molecular weight and steric hindrance around the amide bond. Lower molecular weight compounds, such as **3-6**, **3-16** and **3-18,** are stable in mouse plasma (> 86% remained after four hours) regardless of the left hand acetamide structures. However, the larger compound **3-20**, which has the less sterically hindered di-fluorocyclohexane acetamide, was unstable in mouse plasma (30% remained after four hours). By comparison, compound **3-22**, in which the α-carbon of the acetamide is blocked by the methylene of the cyclopropane ring, is more stable (69% remained after four hours).

The stability of these compounds in mouse liver microsomes (MLM) remained suboptimal and in particular, deuteride blocking at the benzylic position of **3-6** ($T_{1/2}$ = 9 min) had minimal impact

on the microsomal stability (**3-16,** $T_{1/2}$ = 11 min). To better understand the oxidative metabolic pathways in mice, we carried out additional studies of mouse liver microsomes that revealed 3A4 as the major P450 cytochrome isoform responsible for metabolism of these compounds (data not shown). Consistent with this finding, the presence of the CYP3A4 inhibitor ritonavir (3 μM), which is approved for clinical use as a booster of anti-HIV drugs,[22] increased the stabilities of **3-16** ($T_{1/2}$ > 120 min) and **3-18** ($T_{1/2}$ =91 min) in mouse liver microsomes by 10- to 30-fold. The salutary effect of ritonavir was also conferred on derivatives such as **3-22** and **3-25** that contain the benzyl moiety. Ritonavir does not inhibit VSV EBOV infection (IC_{50} > 25 μM), and thus is not expected to confound the evaluation of lead NPC1 inhibitors as anti-EBOV agents. As with **3.47**, **3-21**, **3-23** and **3-24**, the concentration of each of these inhibitors required to reduce cell viability by 50% exceeded 10 μM.

Table 10. *In vitro* ADME properties of selected compounds.

No.	Kinetic solubility (μM)	Mouse PPB (% bound)	Mouse plasma stability (% at 4 hours)	MLM T1/2 (min)	MLM, T1/2 (min) (ritonavir 3 μM)	HLM T1/2 (min)
1a-8	5	99.7	37	1	-	-
2-3	-	-	-	1	-	-
3-6	> 100	86.9	94	9	-	27
3-16	93	-	86	11	> 120	32
3-18	78	87.9	88	3	91	16
3-20	-	-	30	-	> 120	-
3-22	10	97.6	69	-	> 120	-
3-25	4	99.8	72	2	87	1

At this stage, we investigated whether the *in vitro* optimization of **3.47** along with the protective effect of ritonavir would translate into an acceptable pharmacokinetic profile *in vivo*. Oral pharmacokinetic properties for selected compounds were obtained in mice (**Table 11)**.

Table 11. Oral pharmacokinetic parameters for selected compounds in mice.

No.	Dose	T_{max} (hr)	C_{max} (μM)	C@12hr (μM)	AUC_{last} (μM.hr)	$T_{1/2}$ (hr)	Cl_obs (mL/min/Kg)
3-16	25 mg/kg	0.6	7.2	0.2	19.9	2.3	49.0

3-16/ ritonavir	25mg/kg/ 20mg/kg	1.3	12.0	1.7	76.8	2.3	12.3
3-18/ ritonavir	50mg/kg/ 50mg/kg	1.7	19.5	2.0	120.9	3.2	15.5
3-22/ ritonavir	50mg/kg/ 50mg/kg	4.0	10.4	4.7	116.4	2.2	11.9
3-25/ ritonavir	50mg/kg/ 50mg/kg	7.3	7.4	5.7	107.5	1.7	12.5

After administration to mice by gavage, the inhibitor **3-16** was rapidly absorbed and reached a C_{max} of 7.2 μM but was nearly completely cleared in 12 hours. Co-administration of ritonavir (20 mpk) increased the AUC and decreased the clearance of **3-16** by nearly 4-fold. As a result, the plasma concentration of **3-16** after 12 hours increased to 1.7 μM. The pharmacokinetics of a single 50 mpk dose of **3-18**, **3-22** and **3-25** co-administered with ritonavir (50 mpk) was also studied. The plasma concentrations of **3-22** (4.7 μM) and **3-25 (**5.7 μM) after 12 hours were 50-fold greater than the *in vitro* IC_{50}s of these compounds measured against rVSV EBOV infection in 50% human serum **(Table 8).** Not surprisingly, when the concentration of ritonavir decreased after 12 hours, the plasma concentration of the inhibitors declined more rapidly. These findings suggest that an oral b.i.d dosing regimen that delivers an effective concentration of EBOV inhibitors **3-22** and **3-25** can be achieved in mice.

CONCLUSIONS

EBOV infection is initiated by fusion of the virus membrane to target cells. Virus membrane fusion is mediated by a conformational change in the GP that is triggered upon binding to the lysosome membrane protein NPC1.[12] Previous studies identified specific adamantane dipeptide piperazines that inhibit infection by targeting NPC1 and preventing binding and activation of GP. We report here the property-driven lead optimization of this class of inhibitors. Undesirable ADME properties in the original lead compound **3.47** included high hydrophobicity (cLogP = 7.2), attributable in large part to the adamantane, and hydrolyzable amide and methyl ester bonds. SAR efforts identified acceptable replacements for the adamantane with spiro-cyclopropane di-fluoro cyclohexanes and for the ester with methyl sulfone. In addition, we found that halide substitutions at the 5-position of phenyl ring 1 increased potency by almost 10-fold. Those modifications, when combined into a single molecule, resulted in inhibitors, such as **3-**

22 and **3-25,** that are more potent and less hydrophobic than **3.47** and are highly active against EBOV Mayinga (1976), Kikwit (1995) and Makona (2014) that caused the three largest outbreaks of human infection. Compounds **3-22** and **3-25** are stable in mouse plasma for up to 4 hours. It is important to note that the potencies of **3-22** and of **3-25** were reduced by only 5-fold when tested in media containing 10% fetal bovine serum and 50% normal human serum. Furthermore, 3A4 was identified as the major cytochrome P450 isoform that metabolizes these compounds. Consistent with this finding, oral co-administration of either **3-22** or **3-25** to mice with ritonavir, a cytochrome P450-3A4 (CYP3A4) inhibitor with wide clinical use as a booster for anti-virals, resulted in plasma concentrations of **3-22** and **3-25** at 12 hours post dose that are 50-fold greater than the anti-viral IC_{50} of these compounds measured in high serum. These findings suggest that oral b.i.d dosing regimens of **3-22** or **3-25** will deliver effective inhibition of the EBOV receptor function of NPC1 in mice. Selected compounds from this study will be tested in the mouse model of Ebola infection, and those results will be reported in due course.

EXPERIMENTAL SECTION

Chemistry. 1H NMR spectra were recorded on a Varian Inova 600 MHz spectrometer with chemical shifts reported in parts per million (ppm) relative to an internal standard (trimethylsilane). Coupling constants (*J*) are reported in hertz (Hz). Standard resolution mass spectra were obtained on an Agilent 1200 Series HPLC (4.6 x 100 mm, 5 μm Phenomenex C18 reverse-phase column) and a 6130 Series mass spectrometer system; all mass spectra were obtained using electrospray ionization (EI) in positive ion mode. Standard reverse-phase HPLC conditions were as follows: mobile phase A = 0.1% formic acid in water; mobile phase B = 0.1% formic acid in acetonitrile. The same standard reverse-phase HPLC conditions were also used to determine the purity of the synthesized compounds. For singletons, all compounds have purities > 95%. All libraries compounds (parallel syntheses, **1b-1** to **1b-18**) have purities > 90%. Solvents for synthesis were purchased as anhydrous grade and used without further purification. Reagents were purchased from commercial sources and used as received.

General synthetic procedure for the preparation of 1a-2, 1a-5 to 8, 1a-10 to 17 (Scheme 1).

To a mixture of the appropriate acid (**12**, 3.2 mmol, 1 eq), tert-butyl glycinate (**13**, 3.9 mmol, 1.2 eq), HATU (4.8 mmol, 1.5 eq), under nitrogen was added 6 mL of anhydrous DMF. Under stirring, N, N-diisopropylethylamine (0.3 mL) was added and the reaction then stirred for

overnight at room temperature. To the mixture was added water (30 mL) and a white wax precipitate formed. The water was decanted, and the precipitate was washed with water (3 x 30 mL) under sonication, then dried to afford crude product of **14,** which was used without further purification.

In a glass vial, the substituted tert-butyl glycinate **14** (2 mmol) was dissolved in 2 mL of EtOAc and then 2 mL of 4 N HCl in dioxane was added to the solution. The mixture was stirred at room temperature for overnight and then concentrated by GeneVac. The desired acid **11** was obtained as a solid, and used without further purifications.

To a mixture of proper phenol aldehyde (**4**, 3.8 mmol, 1eq) and potassium carbonate (11 mmol, 3 eq) in DMF (5 mL) was added 1-(bromomethyl)-4-substituted benzene (**5**, 4.0 mmol,1.05 eq) and the resulting mixture was stirred for 16 h at room temperature. The solvent was removed under reduced pressure, and the residue was partitioned between H_2O (20 mL) and EtOAc (50 mL). The organic layer was washed with brine, dried over sodium sulfate, and concentrated under reduced pressure. The residue was purified by flash column chromatography (gradient: 20-100% EtOAc/hexanes) to give **6** as a white solid,

In a vial was placed piperazine **7** (0.06-0.15 mmol, 1.2 to 3 eq, and for the preparation of **7**, please refer to **scheme 5**) in 2 mL of anhydrous DME or DCM. Aldehyde **6** (0.05 mmol, 1 eq) was then added, followed by $NaBH(OAc)_3$ (0.1-0.2 mmol, 2 to 4 eq) at 0 ^oC. The reaction was allowed to warm to rt, and stirred for overnight, and then was dried to afford an oily crude mixture. To this mixture was added sat. aq.Na_2CO_3 (5 mL), and the suspension was sonicated for 10 minutes to obtain a sticky brown color wax/oil. The wax/oil was further sonicated with water (2 x 10 mL). The waxy residue was then dried to afford the crude products. Pure compounds **1a-2**, **1a-5** to **8**, **1a-10** to **17** were then obtained by preparative thin layer chromatography (5% MeOH/CH_2Cl_2).

2-((3r,5r,7r)-Adamantan-1-yl)-N-(2-oxo-2-(4-(2-((4-sulfamoylbenzyl)oxy)benzyl)piperazin-1-yl)ethyl)acetamide (1a-5). Yield: 54.0%. ^{1}H NMR (400 MHz, Chloroform-*d*, ppm) δ: 7.95 (d, *J* = 8.4 Hz, 2H), 7.58 (d, *J* = 8.4 Hz, 2H), 7.34 (dd, *J*1 = 7.4 Hz, *J*2 = 1.7 Hz, 1H), 7.27 - 7.23 (m, 3H), 6.99 (td, *J*1 = 7.4 Hz, *J*2 = 1.0 Hz, 1H), 6.92(d, *J* = 8.2 Hz, 1H), 6.49 (t, *J* = 3.8 Hz, 1H), 5.16 (s, 2H), 4.02 (d, *J* = 4.0 Hz, 2H), 3.63 - 3.59 (m, 4H), 3.36 (t, *J* = 4.9 Hz, 2H), 2.47 - 2.42 (m, 4H), 2.01 (s, 2H), 1.96 (s, 3H), 1.70- 1.60 (m, 12H). MS: m/z 595.30 $[M + H]^+$, calc'd for $C_{32}H_{43}N_4O_5S$: 595.29.

2-((3r,5r,7r)-Adamantan-1-yl)-N-(2-(4-(2-((4-(N-methylsulfamoyl)benzyl)oxy)benzyl)piperazin-1-yl)-2-oxoethyl)acetamide (1a-6). Yield: 65.7%. ^{1}H NMR (400 MHz, Chloroform-*d*, ppm) δ: 7.92 - 7.89 (m, 2H), 7.61 (d, *J* = 8.4 Hz, 2H), 7.38 (dd, *J*1 = 7.6 Hz, *J*2 = 1.6 Hz,1H), 7.28 - 7.24 (m, 1H), 7.02 - 6.91 (m, 2H), 6.55 (t, *J* = 3.6 Hz, 1H), 5.17 (s, 2H), 4.07 (d, *J* = 4.0 Hz, 2H), 3.65 (d, *J* = 7.6 Hz, 4H), 3.49 (s, 1H), 3.43 (t, *J* = 4.8 Hz, 2H), 2.69 (s, 3H), 2.51 (t, *J* = 4.8 Hz, 4H), 2.02 (s, 2H), 1.97 (s, 3H), 1.71 - 1.63 (m, 12H). MS: m/z 609.17 $[M + H]^+$, calc'd for $C_{33}H_{45}N_4O_5S$: 609.31.

Additional synthetic procedures and chemical data for compounds **1a-2**, **1a-7** and **8, 1a-10** to **1a-17** are available in Supporting Information.

General synthetic procedure for the preparation of 1b-1 to 1b-18 (Scheme 5).

To a mixture of the 2-adamantan-1-yl acetic acid (**12-1**, 2.4 mmol, 1.2 eq), tert-butyl 4-glycylpiperazine-1-carboxylate **23** (2 mmol, 1 eq), and HATU (3 mmol, 1.5 eq) under nitrogen was added 4 mL of anhydrous DMF. Under stirring, N, N-diisopropylethylamine (1 mL) was added, and the reaction then stirred for overnight at room temperature. To the mixture was added water (30 mL), and a white waxy precipitate formed. The water was decanted, and the residue washed with water (3 x 30 mL) under sonication and then dried to afford **24,** which was used without further purification.

In a 5mL glass vial, the Boc-protected piperazine **24** (1 mmol) was dissolved in 1 mL of EtOAc and then 1 mL of 4 N HCl in dioxane was added. The mixture was stirred at room temperature for overnight and then concentrated by GeneVac. The HCl salt of piperazine **7** was obtained as a solid and was used without further purification.

In a vial was placed piperazine **7** (0.05 mmol, 1eq) in 2 mL of anhydrous DCM. Aldehydes **26** (0.06 mmol, 1.2eq) was then added, followed by $NaBH(OAc)_3$ (0.2 mmol, 4 eq). The reactions were placed on a shaker for overnight and then dried in Genevac to afford oily crude mixtures. To each of these crude mixtures were added 2 mL of sat. aq. Na_2CO_3, and these mixtures were then sonicated for 10 minutes, to get suspensions. After centrifugation, the water was removed, and the solid residue at the bottom of each vial was washed with water (2 mL), and dried, to afford the crude products. Each crude product was further purified using acid-functionalized silica gel (Silica-$PhSO_3H$) column to afford **1b-1** to **1b-18**. LCMS indicated that each one of compounds **1b-1** to **1b-18** was with the correct molecular weight, and was in greater than 90% purities.

General synthetic procedure for the preparation of 2-1 to 2-18 (Scheme 6).

In a vial was placed Boc-piperazine (**8**, 2 mmol, 1.1 eq) in 5 mL of anhydrous DCM. Appropriate aldehyde **6** (1.85 mmol, 1 eq) was then added, followed by $NaBH(OAc)_3$ (3.7 mmol, 2 eq) at 0 ^oC. The reaction was allowed to warm to rt, stirred for overnight and then was dried under reduced pressure to afford an oily crude mixture. To this crude mixture was added sat. aq. Na_2CO_3, and the suspension was sonicated for 10 minutes, to get a sticky brown color wax/oil, which was further sonicated with water (2 x 10 mL). The residue was dried to afford crude **27**, which was used without further purification.

In a 5 mL glass vial, the Boc-protected piperazine **27** (2 mmol) was dissolved in 2 mL of EtOAc and then 2 mL of 4 N HCl in dioxane was added. The mixture was stirred at room temperature for overnight and then concentrated by GeneVac. The HCl salt of piperazine **28** was obtained as a solid, which was used without further purification.

To a mixture of (tert-butoxycarbonyl)glycine **29**, (1.2 mmol, 1.2 eq), piperazine **28** (1 mmol, 1eq), HATU (1.5 mmol, 1.5 eq) was added 3 mL of anhydrous DMF. Under stirring, N, N-diisopropylethylamine (0.2 mL) was added, and the reaction was then stirred for overnight at room temperature. To the mixture was added water (10 mL), and a white precipitate formed. After sonication and centrifugation, the water was decanted, and the residue was washed with water (1 x 10 mL) under sonication one more time to afford **30**, which was used without further purification.

In a 5 mL glass vial, the Boc-protected amine **30** (1 mmol) was dissolved in 1 mL of EtOAc and then 1 mL of 4 N HCl in dioxane was added. The mixture was stirred at room temperature for overnight and then the mixture was concentrated by GeneVac. The HCl salt of amine **31** was obtained, which was used without further purification.

In a glass vial, the appropriate acid (**12**, 0.1 mmol, 1 eq), amine **31** (0.1 mmol, 1 eq) and HATU (0.12 mmol, 1.2 eq), were dissolved in DMF (0.5 mL) and then DIEA (0.15 mL) was added to the solution. Under N_2 protection, the mixture was stirred at room temperature for overnight then the low boiling point components, such as DIEA were evaporated by GeneVac. Water was then added to the residue, and an oily wax or solid precipitate formed. After sonication and centrifugation, the water phase was removed, and the residue was dissolved in EtOAc, dried by MgSO4, filtered and concentrated under reduced pressure. Pure compounds **2-1** to **2-18** was then obtained by preparative thin layer chromatography (5% $MeOH/CH_2Cl_2$).

N-(2-(4-(2-((4-bromobenzyl)oxy)benzyl)piperazin-1-yl)-2-oxoethyl)-2-((1s,3s,5R,7S)-3-chloroadamantan-1-yl)acetamide (2-1). Yield: 48.8%. ^{1}H NMR (400 MHz, Chloroform-*d*, ppm) δ: 7.51 (d, *J* = 8.0 Hz, 2H) 7.35-7.29(m, 3H), 7.23 (t, *J* = 8.0 Hz, 1H), 6.97 (t, *J* = 4.0 Hz, 1H), 6.90 (d, *J* = 8.0 Hz, 1H), 6.51 (s, 1H), 5.03 (s, 2H), 4.03 (d, *J* = 4.0 Hz, 2H), 3.63 (t, *J* = 8.0 Hz, 2H), 3.62(s, 2H), 3.38 (t, *J* = 8.0 Hz, 2H), 2.48(t, *J* = 8.0 Hz, 4H), 2.19 (s, 2H), 2.10 –2.01 (m, 8H), 1.65–1.53 (m, 6H). MS m/z: 628.30 $[M + H]^+$, calc'd for $C_{32}H_{40}BrClN_3O_3$: 628.19.

2-((1s,3s,5R,7S)-3-bromoadamantan-1-yl)-N-(2-(4-(2-((4-bromobenzyl)oxy)benzyl)piperazin-1-yl)-2-oxoethyl)acetamide (2-2). Yield: 37.5%. ^{1}H NMR (400 MHz, Chloroform-*d*, ppm) δ: 7.51 (d, *J* = 8.0 Hz, 2H) 7.35 - 7.21 (m, 4H), 6.97 (t, *J* = 4.0 Hz, 1H), 6.90 (d, *J* = 8.0 Hz, 1H), 6.50 (s, 1H), 5.03 (s, 2H), 4.03 (d, *J* = 4.0 Hz, 2H), 3.63 (t, *J* = 8.0 Hz, 2H), 3.62(s, 2H), 3.38 (t, *J* = 8.0 Hz, 2H), 2.48 (t, *J* = 8.0 Hz, 4H), 2.20(s, 2H), 2.09 (s, 2H),1.69- 1.52 (m, 12H). MS m/z: 672.20 $[M + H]^+$, calc'd for $C_{32}H_{40}Br_2N_3O_3$: 672.14.

Additional synthetic procedures and chemical data for compounds **2-3** to **2-18** are available in supporting information.

General synthetic procedure for the preparation of 3-1 to 3-7, 3-10 to 3-13 (Scheme 7). These compounds were prepared as depicted in **Scheme 7** using the same standard procedures for the preparation of **compounds 1-** and **2-series** as described above.

N-(2-(4-(5-Chloro-2-hydroxybenzyl)piperazin-1-yl)-2-oxoethyl)-2-(4,4-difluorocyclohexyl)acetamide (3-1). Yield: 25.3%. ^{1}H NMR (400 MHz, Chloroform-*d*, ppm) δ: 7.14 (dd, *J*1 = 8.6 Hz, *J*2 =2.6 Hz, 1H), 6.96 (d, *J* = 2.6 Hz, 1H), 6.77 (d, *J* = 8.6 Hz, 1H), 6.53 (t, *J* = 4.1 Hz, 1H), 4.06 (d, *J* = 4.1 Hz, 2H), 3.68 (s, 4H), 3.48 (t, *J* = 5.1 Hz, 2H), 2.57 (s, 4H), 2.18 (d, *J* = 7.1 Hz, 2H), 2.10 - 2.02 (m, 2H), 1.83 - 1.63 (m, 4H), 1.39 - 1.25 (m, 3H). MS m/z: 444.20 $[M + H]^+$, calc'd for $C_{21}H_{29}ClF_2N_3O_3$: 444.19.

N-(2-(4-(5-Chloro-3-fluoro-2-hydroxybenzyl)piperazin-1-yl)-2-oxoethyl)-2-(4,4-difluorocyclohexyl)acetamide (3-2). Yield: 26.1%. ^{1}H NMR (400 MHz, Chloroform-*d*, ppm) δ: 7.07 - 7.00 (m, 1H), 6.77 (s, 1H), 6.55 (s, 1H), 4.07 (d, *J* = 4.1 Hz, 3H), 3.74 (s, 4H), 3.50 (t, *J* = 5.1 Hz, 2H), 2.59 (d, *J* = 5.0 Hz, 3H), 2.19 (d, *J* = 7.1 Hz, 2H), 2.13 - 2.03 (m, 2H), 1.85 - 1.62 (m, 4H), 1.40 - 1.27 (m, 3H). MS m/z: 462.20 $[M + H]^+$, calc'd for $C_{21}H_{28}ClF_3N_3O_3$: 462.18.

Additional synthetic procedures and chemical data for compounds **3-3** to **3-25** are available in supporting information.

Solubility. Kinetic solubility was tested from a 10 mM DMSO stock solution by spiking into

pre-warmed pH 7.4 phosphate buffered saline in a 96-well plate. The final concentration was 100 μM (1% DMSO). The plate was maintained at ambient temperature for 24 hours on an orbital shaker. Samples were centrifuged through a Millipore Multiscreen Solvinter 0.45 micron low binding PTFE hydrophilic filter plate and were analyzed by HPLC or LC-MS/MS if additional sensitivity was required. Peak area was compared to standards of known concentration.

Plasma protein binding. Plasma protein binding was determined using equilibrium dialysis using ThermoScientific™ RED Device. The plate was incubated with shaking at 37 ^{o}C for 6 hours. The concentration of drug in the plasma vs buffer compartments were determined by LC-MS/MS. The fraction bound was calculated as ([plasma] – [buffer]) / [plasma].

Plasma stability. Plasma stability was evaluated by incubating 10 μM test compound with undiluted plasma at 37°C with aliquots removed at multiple time points out to four hours. Aliquots were added to acetonitrile (5X, v:v) to stop any enzymatic activity and held on ice. Samples were centrifuged through a Millipore Multiscreen Solvinter 0.45 micron low binding PTFE hydrophilic filter plate and analyzed by LC-MS/MS.

Hepatic microsomal stability. Microsome stability was evaluated by incubating 1 μM test compound with 1 mg/mL hepatic microsomes in 100 mM KPi, at pH 7.4. The reaction was initiated by adding NADPH (1 mM final concentration). Aliquots were removed at 0, 5, 10, 20, 40, and 60 minutes and added to acetonitrile (5X, v:v) to stop the reaction and precipitate the protein. NADPH dependence of the reaction was evaluated by setting up incubations without NADPH. At the end of the assay, the samples were centrifuged through a Millipore Multiscreen Solvinter 0.45 micron low binding PTFE hydrophilic filter plate and analyzed by LC-MS/MS. Data were log transformed and represented as half-life.

Pharmacokinetics. Pharmacokinetics of lead compounds were assessed in C57Bl/6 or BALB/cmice. Blood was collected at representative time points e.g. 0.08, 0.25, 0.5, 1, 2, 4, 8, 12 and 24 hours and pharmacokinetic parameters were calculated using Phoenix WinNonlin®to determine peak plasma concentration (Cmax), oral bioavailability (%F), exposure (AUC), half-life (t1/2), clearance (CL), and volume of distribution (Vd). Compounds were dosed intravenously via the tail vein or by oral gavage. In some cases, co-formulation with Ritonavir was used as a boosting strategy. All procedures are approved by the Scripps Florida IACUC and Scripps vivarium is fully AAALAC accredited.

Cell lines. Vero E6 cells were maintained in DMEM (Invitrogen) containing 10% fetal bovine

serum (FBS, Gemini Bio-Products) and 0.292 mg/mL L-glutamine (Invitrogen).

Production and purification of VSV EBOV and rVSV EBOV virions. VSV pseudotyped viruses were produced as described previously.[19] rVSV EBOV was created by reverse genetics using rVSV-LFV[23] in which the sequence encoding Lassa GP was replaced with EBOV GP. These viruses express an M-GFP fusion protein. rVSV EBOV was amplified by infecting Vero cells at 90% - 95% confluency with 10-fold dilutions of stock in D2 media (2x Modified Eagle Medium supplemented with 4% FBS) at 37°C. After 2 hours, supernatants were removed and cells were overlaid with a 1:1 mixture of D2 media and sterile 2% agarose and incubated at 37°C. 48 hours – 72 hours post-infection, a GFP-positive plaque was picked, dissolved in DMEM + 10% FBS and used to infect Vero cells. 24 hours later, the supernatant was removed, filtered and used to infect fresh Vero cells to amplify the virus. Virus-containing supernatants were harvested when cells exhibited a significant amount of CPE (36 hours – 72 hours post infection), passed through 0.45 μm Supor® membrane filters and frozen at -80°C. An aliquot of frozen rVSV EBOV stock was thawed and Vero cells at 90% – 95% confluency were incubated with 10-fold dilutions in D2 media for 2 hours at 37°C. Supernatants were then removed and cells were overlaid with a 1:1 mixture of D2 media and sterile 1.5% methylcellulose and placed back into 37°C. 48 hours – 72 hours post-infection, the overlay was removed and cells were stained with crystal violet (0.8% in ethanol) for 45 min at 25°C with rocking. After staining, cells were washed to remove excess crystal violet and the number of plaques were counted. rVSV EBOV titer = 7.67×10^6 pfu/mL. All plaques were GFP-positive.

Infection assay to measure inhibitor activity. Vero cells were plated in 96-well plates at 50% confluency the day before infection. Two hours before infection, eight serial dilutions of each inhibitor to be tested were added directly to the cell cultures using the HP D300 digital dispenser in three-fold dilutions starting at 10 μM. The DMSO concentration in each well was normalized to 1% using an HP D300 digital dispenser. VSV EBOV or rVSV EBOV particles (MOI = 0.5) were added to Vero cells and assayed 8 hours – 12 hours later using fluorescence microscopy. An infectious unit (i.u.) is defined as one EGFP-expressing cell after exposure to virus particles such that the number of GFP-positive cells is directly proportional to the virus dilution. IC_{50} values were calculated in GraphPad Prism by fitting to a single-slope dose response curve. Each compound was analyzed at least 3-10 times. For serum shift assay, the inhibitor activity was measured using rVSV EBOV to infect Vero cells cultured in DMEM

(40%), fetal bovine serum (10%) and normal human serum (50%). EGFP–positive cells were counted 8 hours after infection.

Ebola virus infections under BSL-4 conditions. Anti-EBOV assays were conducted in BSL-4 at USAMRIID. HeLa cells were seeded at 2,000 cells per well in 384-well plates. Ten serial dilutions of inhibitor in triplicate were added directly to the cell cultures using the HP D300 digital dispenser in two-fold dilution increments starting at 10 μM at 2 h before infection. The DMSO concentration in each well was normalized to 1% using an HP D300 digital dispenser. The assay plates were transferred to the BSL-4 suite and infected with EBOV Kikwit, Makona or Mayinga at a multiplicity of infection of 0.5 PFU per cell. The assay plates were incubated in a tissue culture incubator for 48 h. Infection was terminated by fixing the samples in 10% formalin solution for an additional 48 h before immune-staining for EboV GP expression. The data is the mean number of GP-positive cells normalized to 100% in the wells treated with DMSO vehicle alone.

AUTHOR INFORMATION

Corresponding Author

*Corresponding author: jcunningham@bwh.harvard.edu

Present Addresses

[§]**Kyungae Lee: Broad Institute, Cambridge MA 02142**

Author Contributions

[#]**Hu Liu and Yi Tien contributed equally to this work**

Funding Sources

This work was supported by NIH/NIAID grant 1U19AI109740 awarded to J.M.C and S.W.

M.K.W. was supported by NIH grant F31AI131452.

Note

The authors do not have any competing interests.

ACKNOWLEDGEMENT

We thank David Scott and John Hatcher for assistance with preparative HPLC and David Scott for review of the manuscript (D.A.S.). We also thank Nathanael Gray for helpful suggestions and Sun-Young Lim for creating the TOC figure.

ABBREVIATIONS

ADME, absorption, distribution, metabolism, and excretion; b.i.d, twice a day; DCM, Dichloromethane; DMF, Dimethylformamide; EtOH, Ethanol; EBOV, Ebola virus; EtOAc, Ethyl Acetate; EDCI, N-(3-Dimethylaminopropyl)-N-ethylcarbodiimide; FBS, fetal bovine serum; GP, glycoprotein; HATU, 1-[Bis(dimethylamino)methylene]-1H-1,2,3-triazolo[4,5-b]pyridinium 3-oxide hexafluorophosphate; HOAt -1-Hydroxy-7-azabenzotriazole; MeOH, Methanol; MLM, mouse liver microsomal; NHS, normal human serum; NPC1, Neimann-Pick C1; iPr2NEt, N,N-Diisopropylethylamine; PPB, plasma protein binding; SAR, structure−activity relationship; THF, Tetrahydrofuran; TLC, thin layer chromatography; VSV, vesicular stomatitis virus.

SUPPORTING INFORMATION

The Supporting Information is available free of charge on the ACS Publications website.
Additional experimental protocols for synthesis and characterization of compounds **1a-2**, **1a-7**, **1a-8**, **1a-10** to **1a-21**, **2-3** to **2-18**, **3-3** to **3-25.**
Molecular formula strings and some data (CSV).

REFERENCES

1. Geisbert, T. W.; Jahrling, P. B. Exotic emerging viral diseases: progress and challenges. *Nat Med* **2004,** 10, S110-121.
2. Sullivan, N.; Yang, Z. Y.; Nabel, G. J. Ebola virus pathogenesis: implications for vaccines and therapies. *J Virol* **2003,** 77, 9733-9737.
3. Holmes, E. C.; Dudas, G.; Rambaut, A.; Andersen, K. G. The evolution of Ebola virus: Insights from the 2013-2016 epidemic. *Nature* **2016,** 538, 193-200.
4. Agua-Agum, J.; Allegranzi, B.; Ariyarajah, A.; Aylward, R.; Blake, I. M.; Barboza, P.; Bausch, D.; Brennan, R. J.; Clement, P.; Coffey, P.; Cori, A.; Donnelly, C. A.; Dorigatti, I.; Drury, P.; Durski, K.; Dye, C.; Eckmanns, T.; Ferguson, N. M.; Fraser, C.; Garcia, E.; Garske, T.; Gasasira, A.; Gurry, C.; Hamblion, E.; Hinsley, W.; Holden, R.; Holmes, D.; Hugonnet, S.; Jaramillo Gutierrez, G.; Jombart, T.; Kelley, E.; Santhana, R.; Mahmoud, N.; Mills, H. L.;

Mohamed, Y.; Musa, E.; Naidoo, D.; Nedjati-Gilani, G.; Newton, E.; Norton, I.; Nouvellet, P.; Perkins, D.; Perkins, M.; Riley, S.; Schumacher, D.; Shah, A.; Tang, M.; Varsaneux, O.; Van Kerkhove, M. D.; Team, W. E. R. After Ebola in west Africa--unpredictable risks, preventable epidemics. *N Engl J Med* **2016,** 375, 587-596.

5. Ren, J.; Zhao, Y.; Fry, E. E.; Stuart, D. I. Target identification and mode of action of four chemically divergent drugs against Ebola virus Infection. *J Med Chem* **2018,** 61, 724-733.

6. Yermolina, M. V.; Wang, J.; Caffrey, M.; Rong, L. L.; Wardrop, D. J. Discovery, synthesis, and biological evaluation of a novel group of selective inhibitors of filoviral entry. *J Med Chem* **2011,** 54, 765-781.

7. Nelson, E. A.; Dyall, J.; Hoenen, T.; Barnes, A. B.; Zhou, H.; Liang, J. Y.; Michelotti, J.; Dewey, W. H.; DeWald, L. E.; Bennett, R. S.; Morris, P. J.; Guha, R.; Klumpp-Thomas, C.; McKnight, C.; Chen, Y. C.; Xu, X.; Wang, A.; Hughes, E.; Martin, S.; Thomas, C.; Jahrling, P. B.; Hensley, L. E.; Olinger, G. G.; White, J. M. The phosphatidylinositol-3-phosphate 5-kinase inhibitor apilimod blocks filoviral entry and infection. *PLoS Negl Trop Dis* **2017,** 11, e0005540.

8. Johansen, L. M.; DeWald, L. E.; Shoemaker, C. J.; Hoffstrom, B. G.; Lear-Rooney, C. M.; Stossel, A.; Nelson, E.; Delos, S. E.; Simmons, J. A.; Grenier, J. M.; Pierce, L. T.; Pajouhesh, H.; Lehár, J.; Hensley, L. E.; Glass, P. J.; White, J. M.; Olinger, G. G. A screen of approved drugs and molecular probes identifies therapeutics with anti-Ebola virus activity. *Sci Transl Med* **2015,** 7, 290ra89.

9. Picazo, E.; Giordanetto, F. Small molecule inhibitors of ebola virus infection. *Drug Discov Today* **2015,** 20, 277-286.

10. Nyakatura, E. K.; Frei, J. C.; Lai, J. R. Chemical and structural aspects of Ebola virus entry inhibitors. *ACS Infect Dis* **2015,** 1, 42-52.

11. Cardile, A. P.; Mayers, D. L.; Bavari, S. Current status of chemically synthesized inhibitors of Ebola virus. *Recent Pat Antiinfect Drug Discov* **2014,** 9, 97-103.

12. Cote, M.; Misasi, J.; Ren, T.; Bruchez, A.; Lee, K.; Filone, C. M.; Hensley, L.; Li, Q.; Ory, D.; Chandran, K.; Cunningham, J. Small molecule inhibitors reveal Niemann-Pick C1 is essential for Ebola virus infection. *Nature* **2011,** 477, 344-348.

13. Lee, K.; Ren, T.; Côté, M.; Gholamreza, B.; Misasi, J.; Bruchez, A.; Cunningham, J. Inhibition of Ebola virus infection: identification of Niemann-Pick C1 as the target by optimization of a chemical probe. *ACS Med Chem Lett* **2013,** 4, 239-243.

14. Carette, J. E.; Raaben, M.; Wong, A. C.; Herbert, A. S.; Obernosterer, G.; Mulherkar, N.; Kuehne, A. I.; Kranzusch, P. J.; Griffin, A. M.; Ruthel, G.; Dal Cin, P.; Dye, J. M.; Whelan, S. P.; Chandran, K.; Brummelkamp, T. R. Ebola virus entry requires the cholesterol transporter Niemann-Pick C1. *Nature* **2011,** 477, 340-343.

15. Wang, H.; Shi, Y.; Song, J.; Qi, J.; Lu, G.; Yan, J.; Gao, G. F. Ebola viral glycoprotein bound to its endosomal receptor Niemann-Pick C1. *Cell* **2016,** 164, 258-268.

16. Gong, X.; Qian, H.; Zhou, X.; Wu, J.; Wan, T.; Cao, P.; Huang, W.; Zhao, X.; Wang, X.; Wang, P.; Shi, Y.; Gao, G. F.; Zhou, Q.; Yan, N. Structural insights into the Niemann-Pick C1 (NPC1)-mediated cholesterol transfer and Ebola infection. *Cell* **2016,** 165, 1467-1478.

17. Lipinski, C. A.; Lombardo, F.; Dominy, B. W.; Feeney, P. J. Experimental and computational approaches to estimate solubility and permeability in drug discovery and development settings. *Adv Drug Deliv Rev* **2001,** 46, 3-26.

18. Hann, M. M.; Keserü, G. M. Finding the sweet spot: the role of nature and nurture in medicinal chemistry. *Nat Rev Drug Discov* **2012,** 11, 355-365.

19. Chandran, K.; Sullivan, N. J.; Felbor, U.; Whelan, S. P.; Cunningham, J. M. Endosomal proteolysis of the Ebola virus glycoprotein is necessary for infection. *Science* **2005,** 308, 1643-5.
20. Gant, T. G. Using deuterium in drug discovery: leaving the label in the drug. *J Med Chem* **2014,** 57, 3595-3611.
21. Benigni, R.; Bossa, C. Structural alerts of mutagens and carcinogens. *Current Computer-Aided Drug Design* **2006,** 2, 169-176.
22. Zeldin, R. K.; Petruschke, R. A. Pharmacological and therapeutic properties of ritonavir-boosted protease inhibitor therapy in HIV-infected patients. *J Antimicrob Chemother* **2004,** 53, 4-9.
23. Jae, L. T.; Raaben, M.; Herbert, A. S.; Kuehne, A. I.; Wirchnianski, A. S.; Soh, T. K.; Stubbs, S. H.; Janssen, H.; Damme, M.; Saftig, P.; Whelan, S. P.; Dye, J. M.; Brummelkamp, T. R. Virus entry. Lassa virus entry requires a trigger-induced receptor switch. *Science* **2014,** 344, 1506-1510.

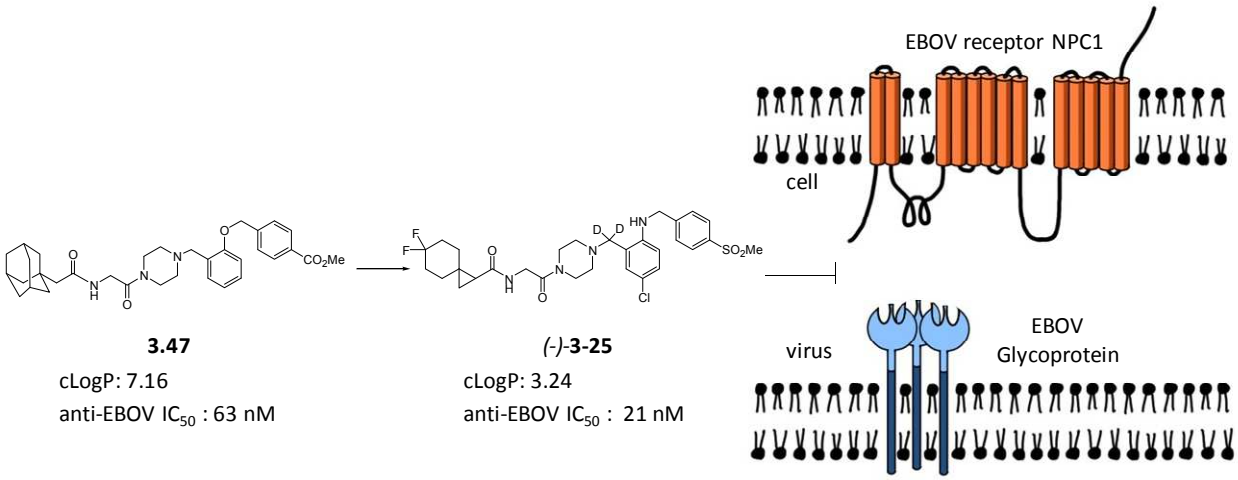

3.47

cLogP: 7.16

anti-EBOV IC_{50} : 63 nM

(-)-**3-25**

cLogP: 3.24

anti-EBOV IC_{50} : 21 nM